SENSOR AND SIMULATION NOTES

NOTE 296

5 JANUARY 1987

RADIATED FIELDS FROM A VERTICALLY-POLARIZED DIPOLE ANTENNA USING AN IMPROVED PULSER/ANTENNA MODEL

Gary D. Sower

EG&G WASC, Inc.

Albuquerque, New Mexico

ABSTRACT

A vertically-polarized dipole antenna is used as a wideband radiator of special waveforms for EMP simulation. The antenna consists of a large right-circular cone with its apex located on the ground. Special resistive loading is used in the antenna so that the current injected into it at the apex decreases linearly with height and becomes zero at the top, maintaining a constant waveform as it travels upward. This particular resistive loading results in an antenna equivalent circuit consisting of the total antenna capacitance in series with its characteristic impedance. The radiation fields are calculated from the antenna current and the total fields are then calculated from the radiation fields. The input current to the antenna is derived from the equivalent circuit of an ideal pulse generator, including the output switch inductance and generator shunt resistance, which give the pulse rise time and late time decay, respectively. The particular model discussed also includes a resistive load in parallel across the antenna input which can be varied to change the late-time waveforms.

I. Introduction

Previous notes[1,2] describe a method of obtaining the fields far away from a resistively-loaded biconical antenna. The calculations are based on a transmission-line model for the antenna, and the antenna itself is approximated by an equivalent dipole antenna. An actual antenna can then be constructed as a suspended biconical structure or as an inverted monocone on a ground plane. A special nonuniform resistive loading was developed which linearly decreases the amplitude of the current with distance along the transmission line, starting with the pulser output current at the antenna apex and becoming identically zero at the top of the cone. This amplitude decrease occurs without change of the wave shape or spectral content as the current propagates. This specific resistive loading also results in a simple antenna equivalent circuit which consists of the total antenna capacitance in series with the characteristic impedance of the transmission line.

An ideal step generator, modeled as a step voltage in series with a generator capacitance (equivalent to a charged capacitor discharging into the antenna through a switch) was used to give the current on the antenna and hence the radiated fields. This simple pulse generator model proved adequate to give reasonable predictions for the measured fields from actual antennas,[3] at least for distances away from the antenna apex greater than its height.

A more realistic model for a pulse generator has been used to give the input voltage to the resistively-loaded antenna.[4] The fields radiated by the resultant current waveform from this model are now derived. In addition, the effect of placing a shunt resistance across the antenna is shown. This resistance can be used to reduce the late-time voltage on the antenna (with a resultant decrease in the late-time electric field) to reduce the possibility of high-voltage breakdown across the pulse generator.

All figures are contained at the end of this report.

II. Summary of Previous Results

The axially symmetric biconical antenna is shown in Figure 1 with the spherical coordinate system used. The characteristic impedance of the bicone is given by

$$Z_c = \frac{Z_o}{\pi} \ln \left[\cot(\theta_o/2)\right] \qquad (1)$$

where

$$Z_o = \sqrt{\mu_o/\varepsilon_o} = 120\pi \tag{2}$$

is the impedance of free space. A dimensionless geometric factor f_g is defined as

$$f_g = \frac{Z_c}{Z_o} = \frac{1}{\pi} \ln \left[\cot(\theta_o/2)\right] \tag{3}$$

The antenna behaves as an ideal transmission line for spherical electromagnetic waves and can be modeled as shown in Figures 2 and 3. Parameters of the transmission line (antenna slant height) are given in terms of the distance ζ along it by

$$L'(\zeta) = \mu_o f_g \tag{4}$$

$$C'(\zeta) = \varepsilon_o / f_g \tag{5}$$

$$Z'(\zeta) = 2\Lambda(\zeta) \tag{6}$$

$\Lambda(\zeta)$ is the special nonuniform resistive loading[1], and is given by

$$\Lambda(\zeta) = \frac{Z_c}{h - |\zeta|} \tag{7}$$

This results in a frequency-domain current $\tilde{I}(\zeta)$ on the antenna

$$\tilde{I}(\zeta) = \tilde{I}(o) \left[1 - \frac{\zeta}{h}\right] e^{-\gamma_o \zeta} \tag{8}$$

A tilde ~ over a quantity indicates the Laplace transform with the variable s. The current starts with amplitude I_o at the antenna apex and decreases linearly with height to zero at the top, maintaining the same waveshape all the way up.

For convenience a normalized retarded time is defined as

$$\tau_h = \frac{ct-r}{h} \tag{9}$$

where

$$c = \frac{1}{\sqrt{\mu_o \varepsilon_o}} = \text{free-space propagation velocity} \tag{10}$$

t = time in seconds

A corresponding normalized (dimensionless) Laplace transform variable is

$$s_h = st_h = s\,\frac{h}{c} \tag{11}$$

where

$$t_h = \frac{h}{c} \tag{12}$$

is the time required for a signal to propagate from the apex to the top of the antenna. The propagation constant on the corresponding lossless transmission line is then

$$\gamma_o = \sqrt{s^2\, L'C'} = \frac{s}{c} = \frac{s_h}{h} \tag{13}$$

$\tilde{I}(o)$ is the current from the generator into the transmission line and is independent of ζ. The voltage along the transmission line is given from the transmission-line equation as

$$\tilde{V}(\zeta) = -\frac{1}{sC'}\,\frac{\partial \tilde{I}(\zeta)}{d\zeta} = -\frac{1}{sC'}\left[-\gamma_o\left(1 - \frac{\zeta}{h}\right) - \frac{1}{h}\right] e^{-\gamma_o \zeta}\, \tilde{I}(o) \tag{14}$$

The input voltage to the line is then

$$\tilde{V}(o) = \frac{1}{sC'h}\left(\gamma_o h + 1\right) \tilde{I}(o) = \frac{1}{sC_a}\left(\gamma_o h + 1\right) \tilde{I}(o) \tag{15}$$

where C_a is the antenna capacitance.

The antenna input impedance is defined by the ratio of the input voltage to input current and is given by

$$Z_a = \frac{\tilde{V}(o)}{\tilde{I}(o)} = \frac{1}{sC_a}\left(\gamma_o h + 1\right) = Z_c + \frac{1}{sC_a} \tag{16}$$

This impedance is the lumped series combination of the lossless biconical antenna characteristic impedance and the total antenna capacitance.

The radiated fields are calculated by assuming that the antenna is very thin, extending from -h to h in Figure 1 as θ_o goes to zero. This approximation can be considered valid in the sense that the spherical fields for $\theta \geq \theta_o$ generated by a current on an infinite bicone are the same as those generated by the same current on an infinite linear dipole. The fact that the current decreases to zero at $\zeta = h$ allows this approximation in the case of the finite bicone. A normalized radiated waveform from this antenna approximation with the current concentrated on the z-axis is calculated as[1]

$$\tilde{\xi}'_i = \sin\theta \frac{\mu_o f_g s_h}{2V_o t_h^2} \int_{-h}^{h} \tilde{I}(z)\, e^{\gamma_o z \cos\theta}\, dz \tag{17}$$

The far-field (radiated) components are given by

$$\tilde{E}_{f_\theta} = \left(\frac{V_o t_h}{2\pi f_g}\right) \frac{e^{-\gamma_o r}}{r} \tilde{\xi}'_i \tag{18}$$

and

$$\tilde{H}_{f_\theta} = \frac{1}{Z_o}\left(\frac{V_o t_h}{2\pi f_g}\right) \frac{e^{-\gamma_o r}}{r} \tilde{\xi}'_i = \frac{1}{Z_o} \tilde{E}_{f_\theta} \tag{19}$$

The near-field components can be calculated[2] from the far-field components to give the total fields as

$$\tilde{E}_\theta = \left(1 + \frac{1}{\gamma_o r} + \frac{1}{\gamma_o^2 r^2}\right) \tilde{E}_{f_\theta} \tag{20}$$

$$\tilde{E}_r = 2 \cot\theta \left(\frac{1}{\gamma_o r} + \frac{1}{\gamma_o^2 r^2}\right) \tilde{E}_{f_\theta} \tag{21}$$

$$\tilde{H}_\phi = \frac{1}{Z_o}\left(1 + \frac{1}{\gamma_o r}\right) \tilde{E}_{f_\theta} \tag{22}$$

The total-field components can be rewritten as

$$\tilde{E}_\theta = \left(\frac{V_o t_h}{2\pi f_g}\right) \frac{e^{-\gamma_o r}}{r} \left[\tilde{\xi}'_1 + \frac{h}{r}\,\tilde{\xi}'_2 + \frac{h^2}{r^2}\,\tilde{\xi}'_3\right] \tag{23}$$

$$\tilde{E}_r = 2 \cot\theta \left(\frac{V_o t_h}{2\pi f_g}\right) \frac{e^{-\gamma_o r}}{r} \left[\frac{h}{r}\,\tilde{\xi}'_2 + \frac{h^2}{r^2}\,\tilde{\xi}'_3\right] \tag{24}$$

$$Z_o \tilde{H}_\phi = \left(\frac{V_o t_h}{2\pi f_g}\right) \frac{e^{-\gamma_o r}}{r} \left[\tilde{\xi}'_1 + \frac{h}{r}\,\tilde{\xi}'_2\right] \tag{25}$$

where $\tilde{\xi}'_2$ and $\tilde{\xi}'_3$ are given by

$$\tilde{\xi}'_2 = \frac{1}{s_h}\,\tilde{\xi}'_1 \tag{26}$$

$$\tilde{\xi}'_3 = \frac{1}{s_h^2}\,\tilde{\xi}'_1 = \frac{1}{s_h}\,\tilde{\xi}'_2 \tag{27}$$

The field components are found in the time domain by obtaining the expression for $\tilde{\xi}'_1$ in the Laplace domain and transforming it to the time domain via the inverse transformation:

$$\xi'_1(t) = \mathcal{L}^{-1}\left[\tilde{\xi}'_1(s)\right] \tag{28}$$

The other normalized field components are obtained by

$$\xi'_2(t) = \mathcal{L}^{-1}\left[\tilde{\xi}'_2(s)\right] = \int_0^\tau \xi'_1(t')\,dt' \tag{29}$$

$$\xi'_3(t) = \mathcal{L}^{-1}\left[\tilde{\xi}'_3(s)\right] = \int_0^\tau \xi'_2(t')\,dt' \tag{30}$$

The total field components are then

$$E_\theta = \left(\frac{V_o}{2\pi f_g}\right)\frac{1}{r}\left[\xi'_1 + \frac{h}{r}\,\xi'_2 + \frac{h^2}{r^2}\,\xi'_3\right] \tag{31}$$

$$E_r = 2\cot\theta\left(\frac{V_o}{2\pi f_g}\right)\frac{1}{r}\left[\frac{h}{r}\,\xi'_2 + \frac{h^2}{r^2}\,\xi'_3\right] \tag{32}$$

$$Z_o H_\phi = \left(\frac{V_o}{2\pi f_g}\right)\frac{1}{r}\left[\xi'_1 + \frac{h}{r}\,\xi'_2\right] = c\,B_\phi \tag{33}$$

III. Pulser Equivalent Circuit

The simplified pulser equivalent circuit, together with that of the antenna, is shown in Figure 4. Also included is a possible shunt resistance R_a across the antenna apex.

The generator capacitance C_g for a typical pulser is the erected capacitance of the Marx generator in parallel with the peaking capacitance. The charging, balancing, and trigger resistors form a finite shunt resistance R_g across the capacitance. The pulser output rise time is usually determined by by the inductance of the output switch L_s. Higher order terms in the source generator are neglected in this analysis. Such terms include the capacitance across the output switch which causes the prepulse and deviations from the ideal switch firing angle which add reactive terms to the pulser equivalent circuit.

For a source voltage of V_o (erected Marx voltage), the input voltage to the antenna terminals is given by

$$\tilde{V}(o) = V_o \frac{[R_gC_gR_a]+s[R_gC_gR_aC_aZ_c]}{\left\{\begin{array}{c}[R_a+R_g]+s[R_gC_gR_a+R_gC_a(R_a+Z_c)+R_aC_aZ_c+L_s] \\ +s^2[R_gC_gR_aC_aZ_c+L_s(R_gC_g+R_aC_a+C_aZ_c)]+s^3[L_sR_gC_gC_a(R_a+Z_c)]\end{array}\right\}} \quad (34)$$

Without R_a, this reduces to

$$\tilde{V}(o) = V_o \frac{[R_gC_g]+s[R_gC_gC_aZ_c]}{1+s[R_gC_g+R_gC_a+C_aZ_c]+s^2[R_gC_gC_aZ_c+L_sC_a]+s^3[L_sR_gC_gC_a]} \quad (35)$$

The current into the antenna is given by

$$\tilde{I}(o) = \frac{\tilde{V}(o)}{Z_c + \frac{1}{sC_a}} = \tilde{V}(o) \frac{sC_a}{1+sC_aZ_c}$$

$$= \frac{V_o}{Z_c} \frac{s[R_gC_gR_aC_aZ_c]}{\left\{\begin{array}{c}[R_a+R_g]+s[R_gC_gR_a+R_gC_a(R_a+Z_c)+R_aC_aZ_c+L_s] \\ +s^2[R_gC_gR_aC_aZ_c+L_s(R_gC_g+R_aC_a+C_aZ_c)]+s^3[L_sR_gC_gC_a(R_a+Z_c)]\end{array}\right\}} \quad (36)$$

The coefficients of the Laplace variable in these equations can be represented as

$$\tilde{V}(o) = V_o \frac{A + sB}{C + sD + s^2 E + s^3 F} = V_o \frac{A + sB}{F(s+\alpha)(s+\beta)(s+\gamma)} \quad (37)$$

$$\tilde{I}(o) = \frac{V_o}{Z_c} \frac{sB}{C + sD + s^2 E + s^3 F} = \frac{V_o}{Z_c} \frac{sB}{F(s+\alpha)(s+\beta)(s+\gamma)} \quad (38)$$

The coefficients are

$$A = R_g C_g \tag{39}$$

$$B = R_g C_g C_a Z_c \tag{40}$$

$$C = \frac{R_a + R_g}{R_a} = 1 + \frac{R_g}{R_a} \qquad \left[= 1 \text{ without } R_a\right] \tag{41}$$

$$D = \frac{R_g C_g R_a + R_g C_a (R_a + Z_c) + R_a C_a Z_c + L_s}{R_a} = A + R_g C_a \left(1 + \frac{Z_c}{R_a}\right) + C_a Z_c + \frac{L_s}{R_a} \tag{42}$$

$$\left[= A + R_g C_a + C_a Z_c \text{ without } R_a\right]$$

$$E = \frac{R_g C_g R_a C_a Z_c + L_s (R_g C_g + R_a C_a + C_a Z_c)}{R_a} = B + L_s \left(C_g \frac{R_g}{R_a} + C_a + C_a \frac{Z_c}{R_a}\right) \tag{43}$$

$$\left[= B + L_s C_a \text{ without } R_a\right]$$

$$F = L_s R_g C_g C_a \left(1 + \frac{Z_c}{R_a}\right) \qquad \left[= L_s R_g C_g C_a \text{ without } R_a\right] \tag{44}$$

Also note that the product of the antenna capacitance times its characteristic impedance is the propagation time $t_h = C_a Z_c$.

The frequency coefficients α, β and γ are the three roots of the equation

$$\alpha^3 F - \alpha^2 D + \alpha D - C = 0 \tag{45}$$

The first root α can be found by successive approximations: start with a first approximation of $\alpha = 0$, find the next approximation from

$$\alpha = \frac{C}{D - \alpha E + \alpha^2 F} \tag{46}$$

and repeat until α is constant. The other two coefficients are found from

$$\begin{Bmatrix}\beta\\ \gamma\end{Bmatrix} = \left\{\frac{E/F - \alpha}{2} \pm \sqrt{\left(\frac{E/F - \alpha}{2}\right)^2 - \frac{C}{\alpha F}}\right\} \tag{47}$$

Note that α and γ as used here are not the same terms used in the references.

Figures 5, 6 and 7 show the resulting waveforms into the antenna as given by the above equations. The three figures show the same waveform on different time scales to emphasize different parts of the waveform. Also shown on these three figures is the double-exponential waveform - which would occur for both the voltage and current waveform if the antenna equivalent circuit consisted only of its characteristic impedance, i.e., an infinitely long cone without resistive loading.

IV. Normalized Far-Field Waveform

The normalized far-field waveform can now be determined from equations 8 and 17. $\tilde{I}(o)$ is independent of z and can be removed from the integration:

$$\tilde{\xi}'_1 = \sin\theta \frac{\mu_o f_g s_h}{2V_o t_h^2} \tilde{I}(o) \int_{-h}^{h} \left(1 - \frac{|z|}{h}\right) e^{-\gamma_o|z|} e^{\gamma_o z \cos\theta} dz \tag{48}$$

The integration is detailed in Reference 1, with the result

$$\tilde{\xi}'_1 = \sin\theta \frac{\mu_o f_g h s_h}{2V_o t_h^2} \tilde{I}(o) \left\{ \frac{e^{-s_h(1-\cos\theta)} - 1}{s_h^2 (1-\cos\theta)^2} + \frac{1}{s_h(1-\cos\theta)} \right.$$

$$\left. + \frac{e^{-s_h(1+\cos\theta)} - 1}{s_h^2(1+\cos\theta)^2} + \frac{1}{s_h(1+\cos\theta)} \right\} \tag{49}$$

Some of the trigonometric functions can be combined to give

$$\tilde{\xi}'_1 = \sin\theta \frac{\mu_o f_g h}{2V_o t_h^2} \tilde{I}(o) \left\{ \frac{2}{\sin^2\theta} - \frac{2(1+\cos^2\theta)}{s_h \sin^4\theta} \right.$$

$$\left. + \frac{e^{-s_h(1-\cos\theta)}}{s_h(1-\cos\theta)^2} + \frac{e^{-s_h(1+\cos\theta)}}{s_h(1+\cos\theta)^2} \right\} \tag{50}$$

With $\tilde{I}(o)$ given by equation 38, $\tilde{\zeta}_1'$ becomes

$$\tilde{\xi}_1' = \frac{\sin\theta}{2} \frac{t_h\, B/F}{(s_h+\alpha_h)(s_h+\beta_h)(s_h+\gamma_h)} \left\{ \frac{2s_h}{\sin^2\theta} - 2\,\frac{1+\cos^2\theta}{\sin^4\theta} + \frac{e^{s_h(1-\cos\theta)}}{(1-\cos\theta)^2} + \frac{e^{s_h(1+\cos\theta)}}{(1+\cos\theta)^2} \right\} \tag{51}$$

with $\alpha_h = \alpha t_h$, $\beta_h = \beta t_h$ and $\gamma_h = \gamma t_h$.

The inverse Laplace transform to the time domain gives

$$\begin{aligned}
\xi_1' = \frac{\sin\theta}{2} \frac{t_h\, B/F}{(\alpha_h-\beta_h)(\beta_h-\gamma_h)(\gamma_h-\alpha_h)} \Bigg\{ & (\beta_h-\gamma_h) \left[\left(\frac{\alpha_h}{\sin^2\theta} + \frac{1+\cos^2\theta}{\sin^4\theta} \right) 2e^{-\alpha_h\tau_h}\, U(\tau_h) \right. \\
& \left. - \frac{e^{-\alpha_h\tau_h'}\, U(\tau_h')}{(1-\cos\theta)^2} - \frac{e^{-\alpha_h\tau_h''}\, U(\tau_h'')}{(1+\cos\theta)^2} \right] \\
& + (\gamma_h-\alpha_h) \left[\left(\frac{\beta_h}{\sin^2\theta} + \frac{1+\cos^2\theta}{\sin^4\theta} \right) 2e^{-\beta_h\tau_h}\, U(\tau_h) - \frac{e^{-\beta_h\tau_h'}\, U(\tau_h')}{(1-\cos\theta)^2} - \frac{e^{-\beta_h\tau_h''}\, U(\tau_h'')}{(1+\cos\theta)^2} \right] \\
& + (\alpha_h-\beta_h) \left[\left(\frac{\gamma_h'}{\sin^2\theta} + \frac{1+\cos^2\theta}{\sin^4\theta} \right) 2e^{-\gamma_h\tau_h}\, U(\tau_h) - \frac{e^{-\gamma_h\tau_h'}\, U(\tau_h')}{(1-\cos\theta)^2} - \frac{e^{-\gamma_h\tau_h''}\, U(\tau_h'')}{(1+\cos\theta)^2} \right] \Bigg\}
\end{aligned} \tag{52}$$

where $U(\tau_h)$ is the unit step function and

$$\tau_h' = \tau_h - (1-\cos\theta), \quad \tau_h'' = \tau_h - (1+\cos\theta). \tag{53}$$

This expression contains three terms (in the square brackets) which are identical except for the cyclic permutation of α_h, β_h and γ_h. The only time dependence is contained within these terms, so equation 52 can be rewritten as

$$\xi_1' = K[G_\alpha(\tau_h) + G_\beta(\tau_h) + G_\gamma(\tau_h)] \tag{54}$$

where

$$K = \frac{\sin\theta}{2} \frac{t_h \, B/F}{(\alpha_h-\beta_h)(\beta_h-\gamma_h)(\gamma_h-\alpha_h)} \tag{55}$$

and

$$G_\alpha(\tau_h) = (\beta_h-\gamma_h)\left[\left(\alpha_h + \frac{1+\cos^2\theta}{\sin^2\theta}\right)\frac{2e^{-\alpha_h\tau_h}\,U(\tau_h)}{\sin^2\theta}\right.$$

$$\left. - \frac{e^{-\alpha_h\tau_h'}\,U(\tau_h')}{(1-\cos\theta)^2} - \frac{e^{-\alpha_h\tau_h''}\,U(\tau_h'')}{(1+\cos\theta)^2}\right] \tag{56}$$

V. Normalized Near-Field Waveforms

The normalized near-field terms can now be derived from equations 26 and 27 in the Laplace domain:

$$\tilde{\xi}_2' = \frac{\sin\theta}{2} t_h \frac{B/F}{(s_h+\alpha_h)(s_h+\beta_h)(s_h+\gamma_h)}\left\{\frac{2}{\sin^2\theta} - \frac{2(1+\cos^2\theta)}{s_h\sin^4\theta}\right.$$

$$\left. + \frac{e^{-s_h(1-\cos\theta)}}{s_h(1-\cos\theta)^2} + \frac{e^{-s_h(1+\cos\theta)}}{s_h(1+\cos\theta)^2}\right\} \tag{57}$$

$$\tilde{\xi}_3' = \frac{\sin\theta}{2} t_h \frac{B/F}{(s_h+\alpha_h)(s_h+\beta_h)(s_h+\gamma_h)}\left\{\frac{2}{s_h\sin^2\theta} - \frac{2(1+\cos^2\theta)}{s_h^2\sin\theta}\right.$$

$$\left. + \frac{e^{-s_h(1-\cos\theta)}}{s_h^2(1-\cos\theta)^2} + \frac{e^{-s_h(1+\cos\theta)}}{s_h^2(1+\cos\theta)^2}\right\} \tag{58}$$

The corresponding terms can be derived in the time domain from equations 29 and 39

$$\xi_2' = K \int_0^{\tau_h} [G_\alpha(\tau_h) + G_\beta(\tau_h) + G_\gamma(\tau_h)]\, d\tau_h = K[H_\alpha(\tau_h) + H_\beta(\tau_h) + H_\gamma(\tau_h)] \quad (59)$$

$$\xi_3' = K \int_0^{\tau_h} [H_\alpha(\tau_h) + H_\beta(\tau_h) + H_\gamma(\tau_h)]\, d\tau_h = K[J_\alpha(\tau_h) + J_\beta(\tau_h) + J_\gamma(\tau_h)] \quad (60)$$

where

$$H_\alpha(\tau_h) = \int_0^{\tau_h} G_\alpha(\tau_h)\, d\tau_h$$

and

$$J_\alpha(\tau_h) = \int_0^{\tau_h} H_\alpha(\tau_h)\, d\tau_h, \text{ etc.}$$

The calculations need only be done for the α_h term and then applied to the other terms by the cyclic permutation.

The results of the integrations give

$$H_\alpha(\tau_h) = \frac{(\beta_h - \gamma_h)}{(-\alpha_h)} \left\{ \frac{2}{\sin^2\theta} \left[\alpha_h + \frac{1+\cos^2\theta}{\sin^2\theta} \right] \left[e^{-\alpha_h \tau_{h-1}} \right] U(\tau_h) \right.$$

$$\left. - \left[\frac{e^{-\alpha_h \tau_h'}_{-1}}{(1+\cos\theta)^2} \right] U(\tau_h') - \left[\frac{e^{-\alpha_h \tau_h''}_{-1}}{(1+\cos\theta)^2} \right] U(\tau_h'') \right. \quad (61)$$

$$J_\alpha(\tau_h) = \frac{(\beta_h - \gamma_h)}{\alpha_h^2} \left\{ \frac{2}{\sin^2\theta} \left[\alpha_h + \frac{1+\cos^2\theta}{\sin^2\theta} \right] \left[e^{-\alpha_h \tau_{h-1+\alpha_h \tau_h}} \right] U(\tau_h) \right.$$

$$\left. - \left[\frac{e^{-\alpha_h \tau_h'}_{-1+\alpha_h \tau_h'}}{(1-\cos\theta)^2} \right] U(\tau_h') - \left[\frac{e^{-\alpha_h \tau_h''}_{-1+\alpha_h \tau_h''}}{(1+\cos\theta)^2} \right] U(\tau_h'') \right\} \quad (62)$$

VI. Normalized Field Components

The normalized field components in the frequency domain are given by equation 51, 57 and 58. These components are shown in Figure 7 for a baseline

set of pulser and antenna component values. The first break frequency corresponds to the value of α_h; the second break frequency to β_h, and the third to γ_h. In reference 1, the lowest break frequency, which is due to the pulser shunt resistance, does not exist. Neither does the highest break frequency, which is due to the switch inductance. Figure 8 shows the effect of removing these pulser elements from the model; only $\bar{\xi}_1'$ is shown since the other field components can be obtained from it simply by dividing by the frequency.

A very interesting result of this figure is that the effect of the antenna shunt resistor R_a is nearly identical to that which would occur if it were combined with the pulser shunt R_g, at least for values of R_a equal to or higher than R_g. This is because the effect of the output switch inductance L_s occurs at far higher frequencies than that of the shunt resistances for practical pulser component values, so that it is immaterial on which side of the switch the pulser shunt is located. For values of R_a much smaller than R_g, the high frequencies are decreased in addition to the low frequencies, as seen in Figure 9. This is an undesirable effect (increase in rise time) so such low values of an antenna shunt should not be considered. Of course, if R_a is located on the pulser side, then it cannot be distinguished from a change in value of R_g, and hence it is not a distinct circuit parameter. The antenna shunt is thus not an interesting circuit parameter and will be disregarded in all subsequent discussions.

The time domain waveforms of the normalized field components are shown in Figure 10 for $\theta = \pi/2$ (fields on the ground plane). Figure 11 shows the field components at a point above the ground plane. These compare favorably with the general nature of the waveforms of Reference 1, except that the finite rise time due to the output switch inductance is now included, and that ξ_3' will now eventually return to zero at very late times due to the pulser shunt resistance.

VIII. Normalized Radiated Fields

The current waveform into the antenna, equation 36, can be rewritten in normalized form as

$$\bar{I}(o) = \frac{V_o}{Z_c} \frac{b\, s_h}{1 + s_h[1 + b(1+a)] + s_h^2[b + d] + s_h^3[b\, d]} \tag{63}$$

where normalized, dimensionless variables are defined as:

$$a = \frac{C_a}{C_g} = \text{ratio of antenna capacitance to generator capacitance.}$$

$$b = \frac{t_g}{t_h} = \frac{R_g C_g}{Z_c C_a} = \text{ratio of pulser time constant to antenna propagation time.}$$

$$d = \frac{t_s^2}{t_h^2} = \frac{L_s C_a}{(Z_c C_a)^2} = \text{square of the ratio of output switch time constant to antenna propagation time.}$$

All antenna and pulser components are thus redefined in terms of the propagation time up the antenna and the capacitance ratio.

Equation 38 remains the same, with the coefficients redefined according to equation 63:

$$B = b$$
$$C = 1$$
$$D = 1+b\ (1+a)$$
$$E = b+d$$
$$F = d \cdot b$$

The rest of the equations which determine the radiated fields remain in their original form. The total normalized radiated fields in the frequency domain are given by equations 23, 24 and 25 with the normalized field components given by equations 49, 57 and 58. In the time domain they are given by equations 31, 32 and 33 with the field components of equations 54, 56, 61 and 62. These fields are all normalized in amplitude by unitizing the common term

$$E_o = \frac{V_o}{2\pi r\ f_g} = 1 \text{ V/m} \qquad (64)$$

Studies can now be performed to show the effect of the normalized parameters on the fields in the simulation at normalized distances and elevations. A baseline set of parameters was chosen for an example consisting of

$$a = \frac{C_a}{C_g} = 0.3$$

$$b = \frac{t_g}{t_h} = 50$$

$$d = \frac{t_s^2}{t_h^2} = .03$$

$$\frac{x}{h} = 2 = \text{normalized range}$$

$$\frac{z}{x} = .25 = \text{height/range}$$

Figure 12 shows the spectra of the fields for these parameters and Figure 13 shows the waveforms.

Some comments are in order concerning the general nature of these waveforms and spectra. Of foremost importance is the fact that the radiated fields do not have a double-exponential waveshape. The initial rise time is very nearly that of the double exponential, but the principal field components then decay very rapidly and, in fact, become negative at some time less than the propagation time up the antenna. This "zero crossing time" is primarily a function of the antenna height and is relatively insensitive to all other antenna or pulser parameters, including the resistive loading of the antenna. It is inherent in the far-field components of all radiating antennas, including vertically polarized dipoles. The zero crossing time is often used as a specification for the procurement of such antennas for EMP simulation.

The two discontinuities in the slopes of the fields are due to the antenna current becoming zero at the top (first discontinuity) and in the ground plane image (second discontinuity), and occur at the respective propagation times.

The magnetic field becomes zero at a few time constants, consistent with the fact that it does not contain a static field component. The electric field, however, crosses zero again to become positive and then maintains a moderate static level for a very long time. If there were no shunt resistance, this field would exist forever due to the voltage put onto the capacitance of the antenna.

The slight oscillation of the polar electric field due to the two zero crossings becomes a dip in its spectrum at a value of $w \frac{h}{c} = 0.5$ as seen in Figure 12.

Figures 14 and 15 show the variation of the fields as a function of the angle from the horizon, represented here as the measurement point elevation. As the elevation is increased, the radiated fields become more sharply peaked as a symmetrical high frequency spike with a loss of late-time, low-frequency content. The radial electric field grows correspondingly.

Figures 16 and 17 show how the fields vary with distance from the antenna. As the distance increases the near field terms decrease which reduces the low-frequency, late-time components. At distances closer to the antenna than one antenna height, the results presented here become increasingly inaccurate due to the assumptions on which the calculations are based.

Figures 18 and 19 show the effort of the antenna/pulse generator capacitance on the fields. Larger pulser capacitances are seen to give more mid-frequency components, with less undershoot and a larger zero-crossing time. Both very-high and very-low frequencies do not change with the capacitance ratio.

Figures 20 and 21 show the effect of the pulser shunt resistance, represented here as the $R_g C_g / Z_c C_a$ time constant. Low values of this shunt resistance decrease the low-frequency content and reduce the time that the electric field tail stays high.

Figures 22 and 23 show the effect of the inductance of the output switch. Large inductances are seen to significantly decrease the rise time of the radiated fields and the high-frequency content.

REFERENCES

1. Carl E. Baum, Sensor and Simulation Note 81, Resistively Loaded Radiating Dipole Based on a Transmission-Line Model for the Antenna, April 1969.

2. Bharadwaja K. Singaraju and Carl E. Baum, Sensor and Simulation Note 213, A simple Technique for Obtaining the Near Fields of Electric Dipole Antennas from Their Far Fields, March 1976.

3. Joseph C. Giles, John C. Leib, and Gary D. Sower, ATHAMAS Memo 23, Field Mapping Data for ATHAMAS II, March 1979.

4. Bharadwaja K. Singaraju, Carl E. Baum, and John H. Darrah, ATHAMAS Memo Memo 11, Design Improvements Incorporated in ATHAMAS II (Large VPD), January 1976.

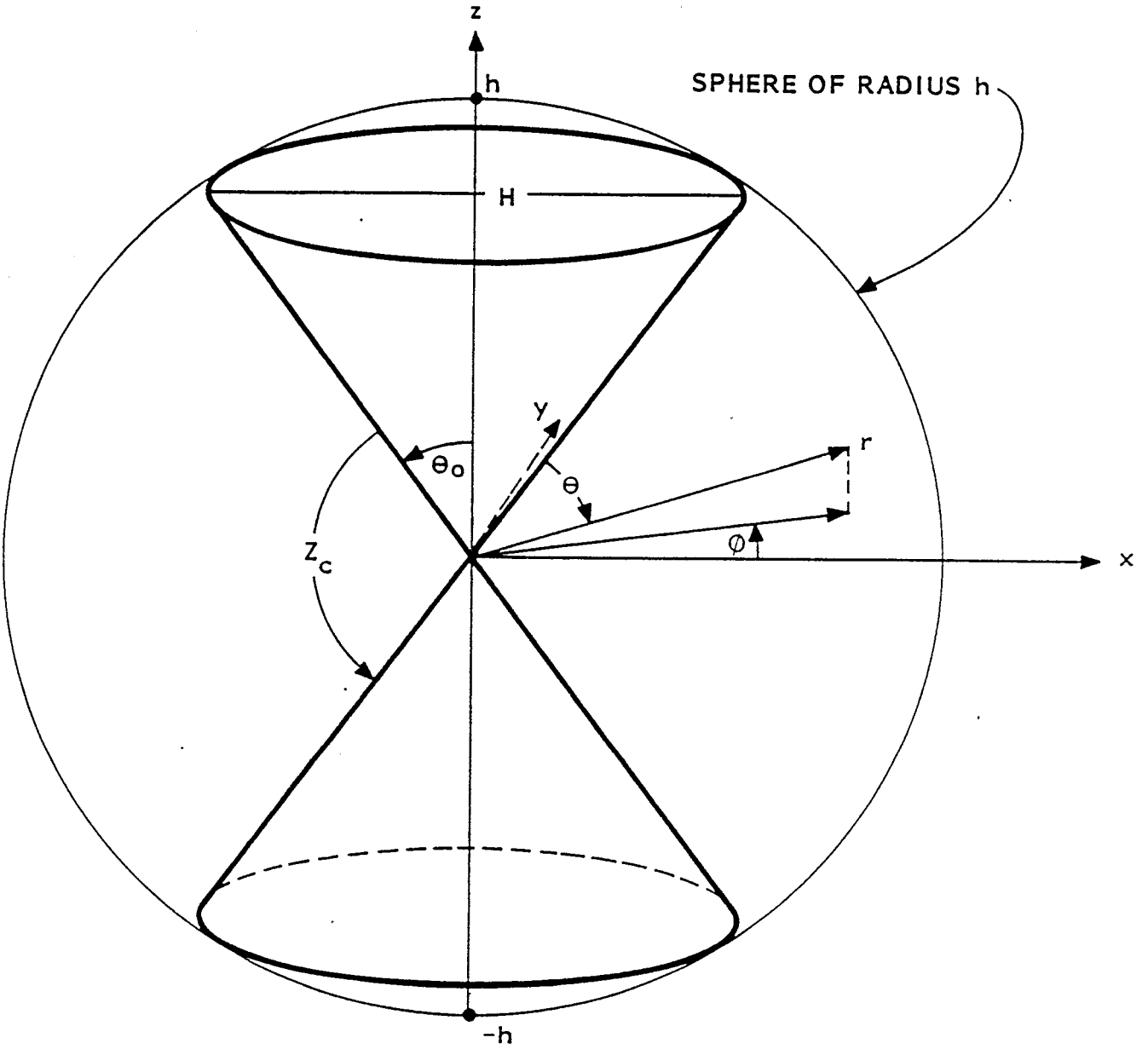

Figure 1. Axially Symmetric Biconical Antenna

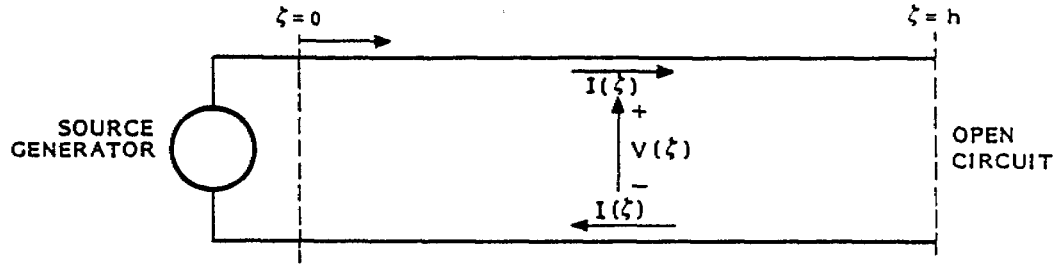

Figure 2. Transmission Line with Generator

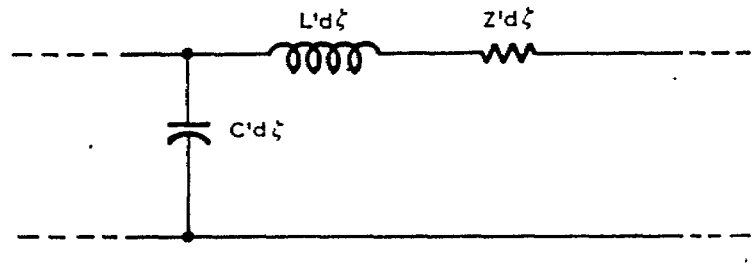

Figure 3. Incremental Section of the Transmission Line

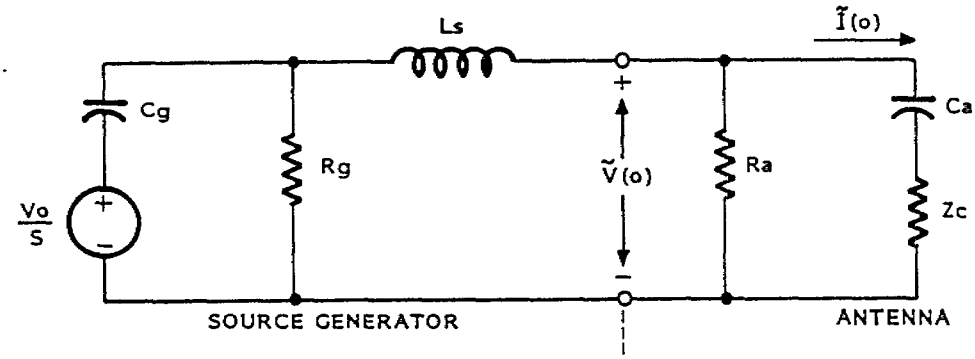

Figure 4. Equivalent Circuit for the Pulser and Antenna

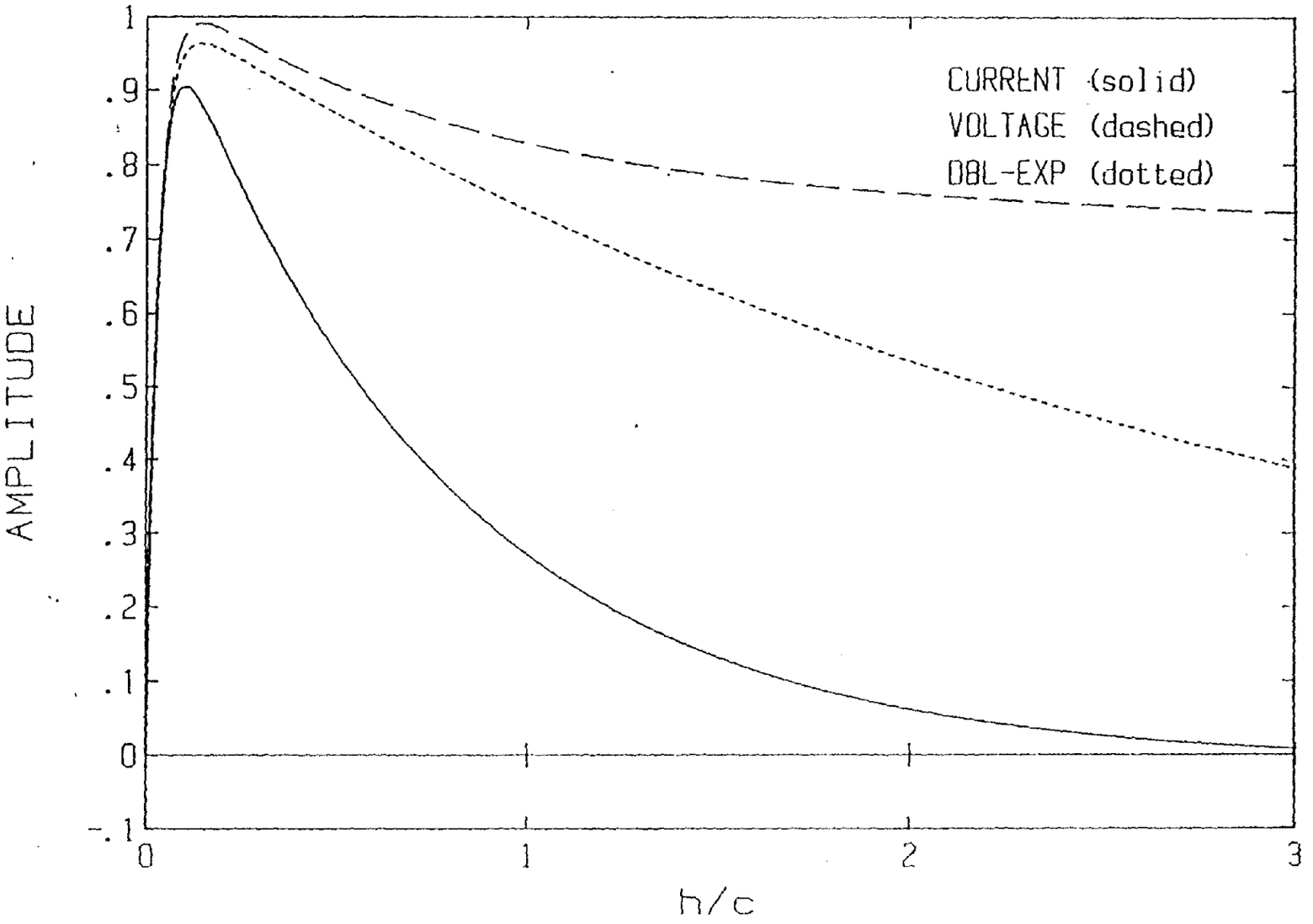

Figure 5. Normalized Waveforms into Antenna - Early Times

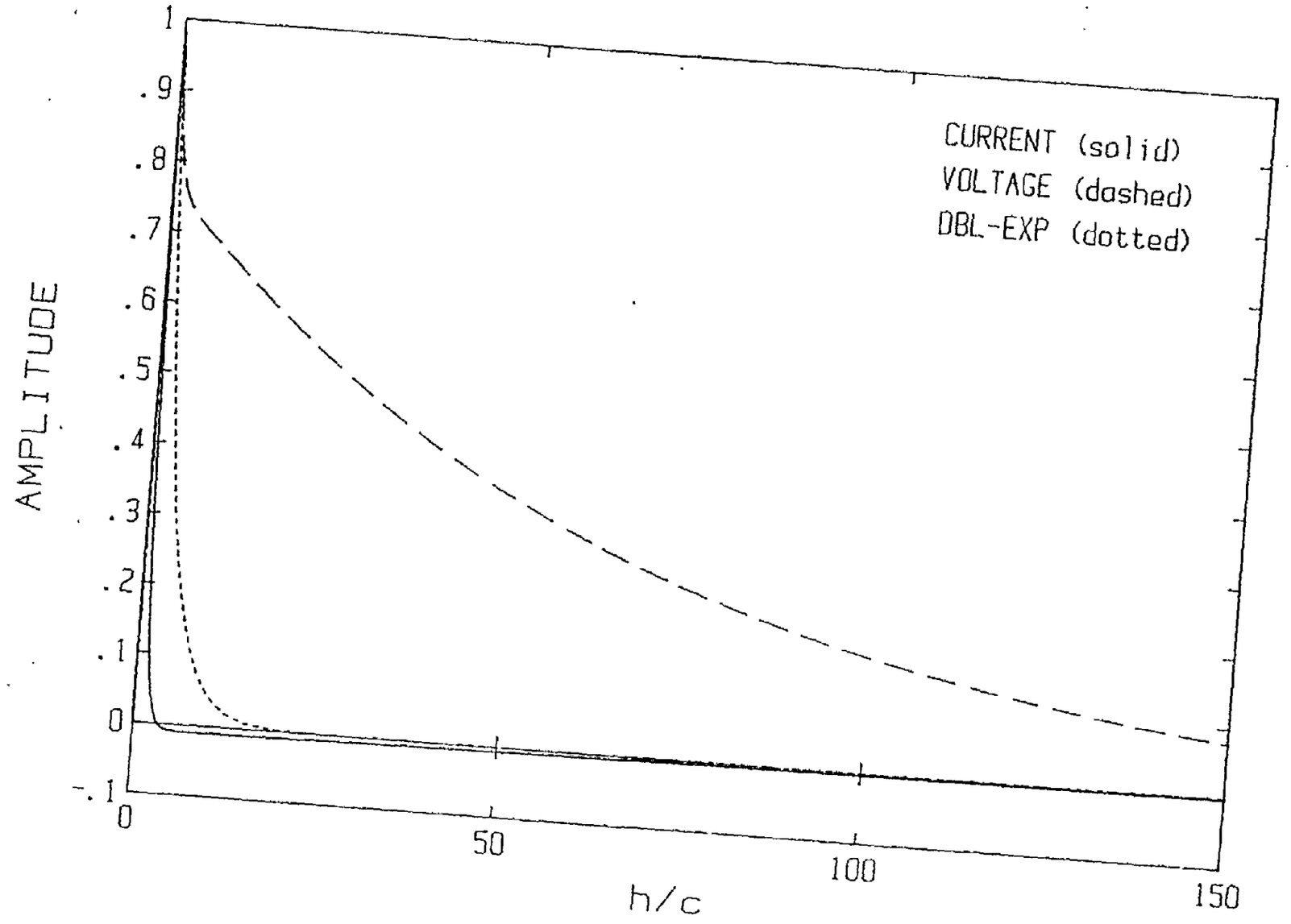

Figure 6. Normalized Waveforms into Antenna - Late Times

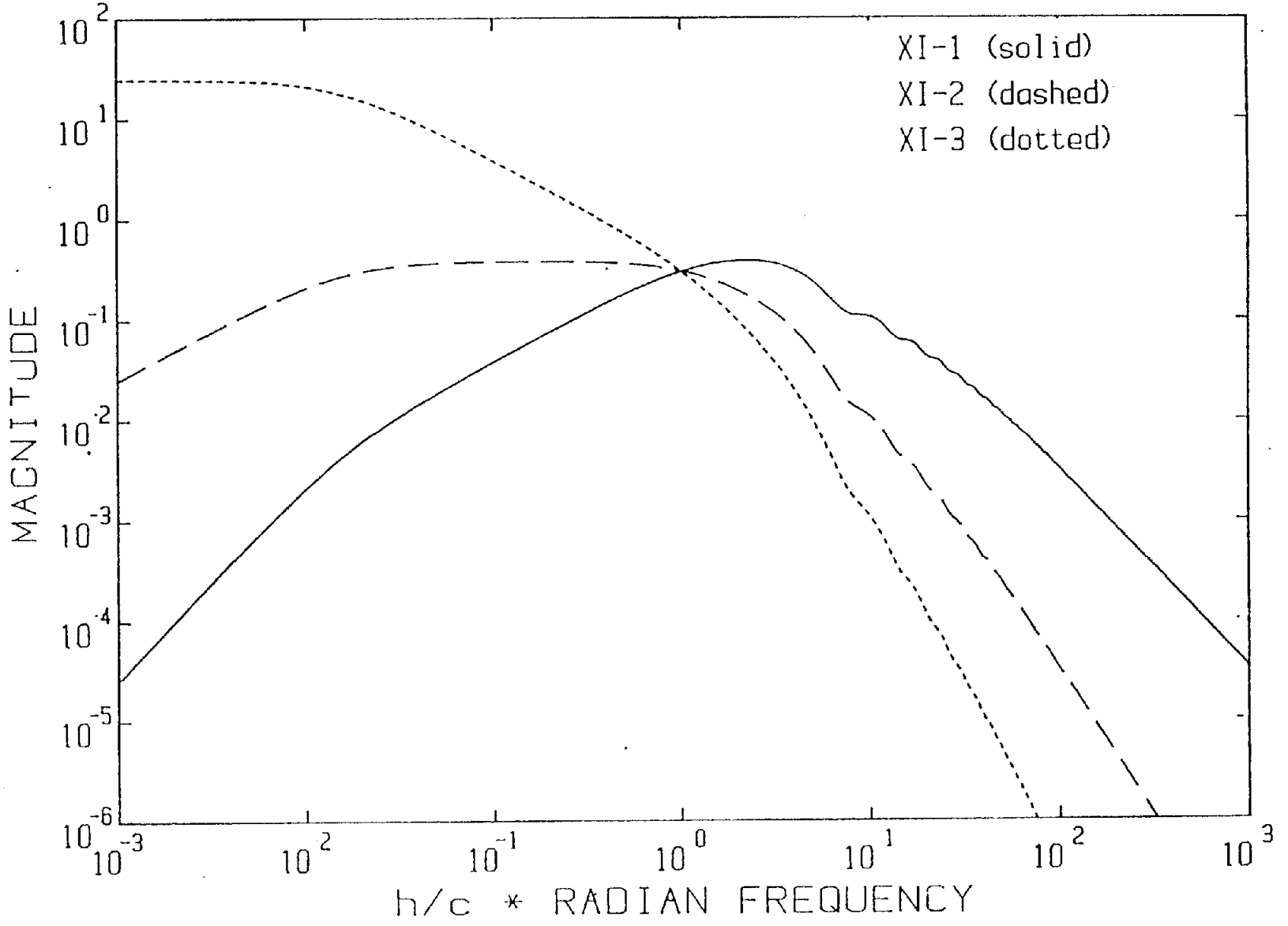

Figure 7. Normalized Field Component Spectra

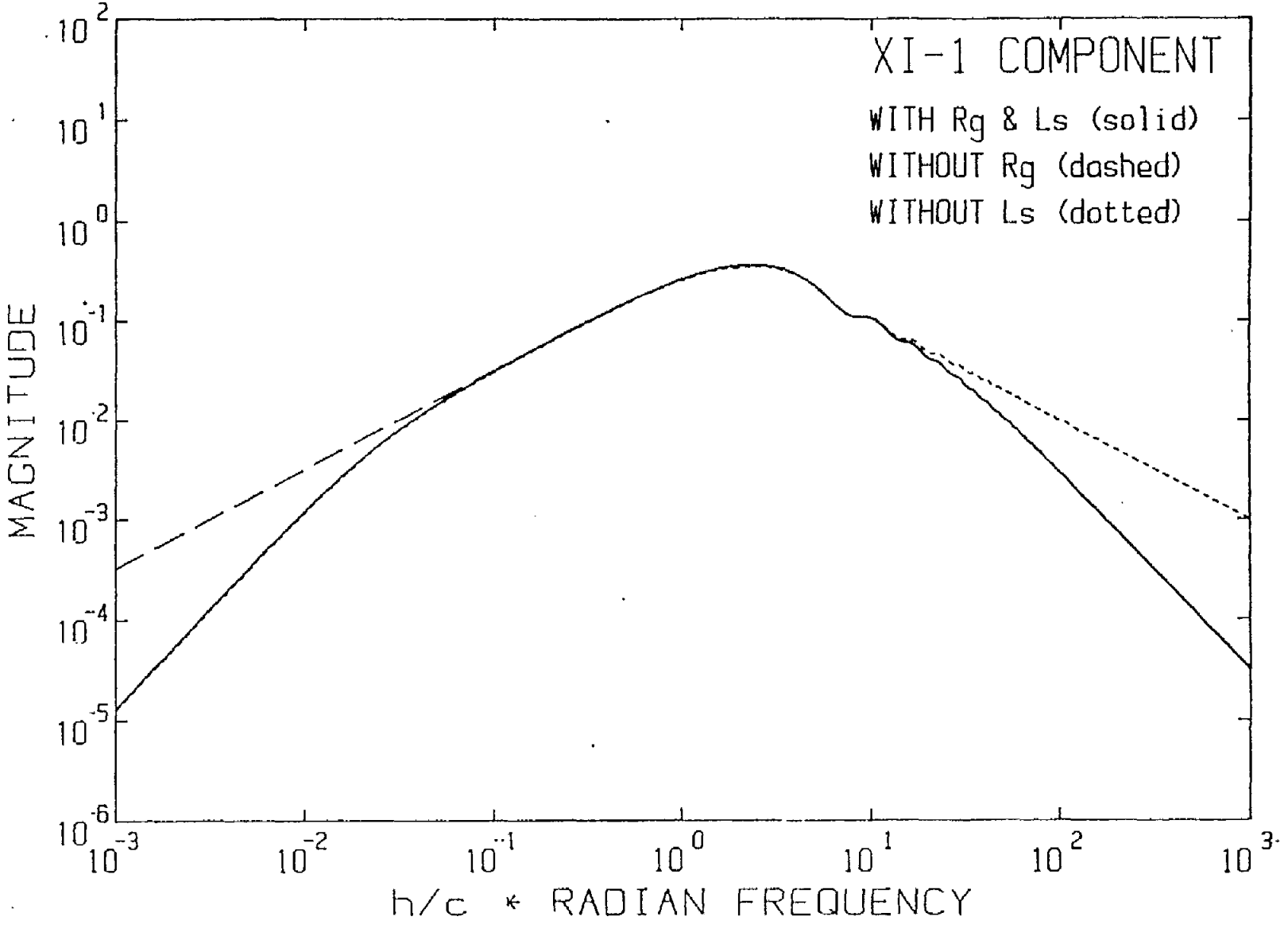

Figure 8. Effect of Pulser Model Without Shunt Resistance and Switch Inductance

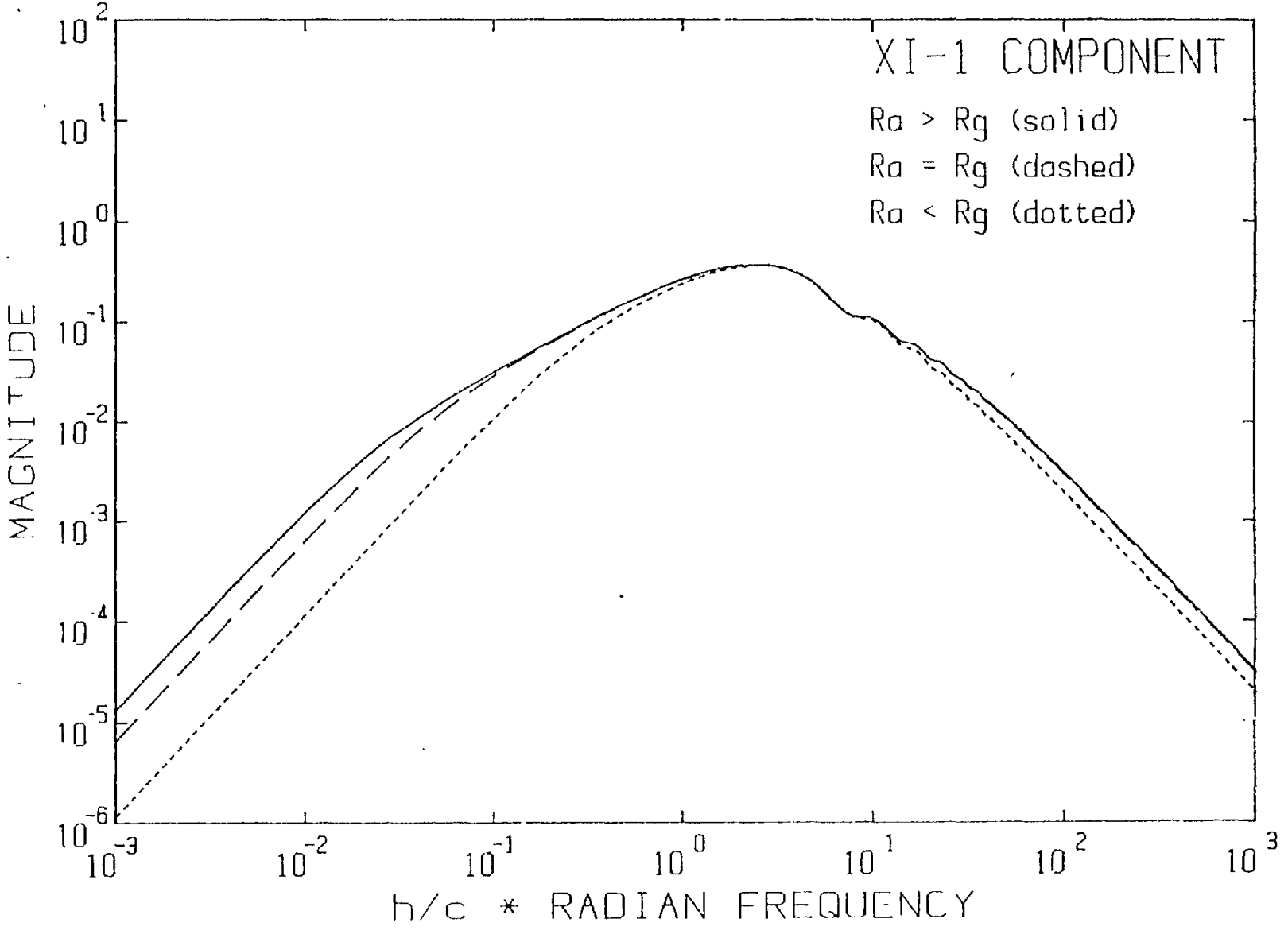

Figure 9. Effect of Antenna Shunt Resistance

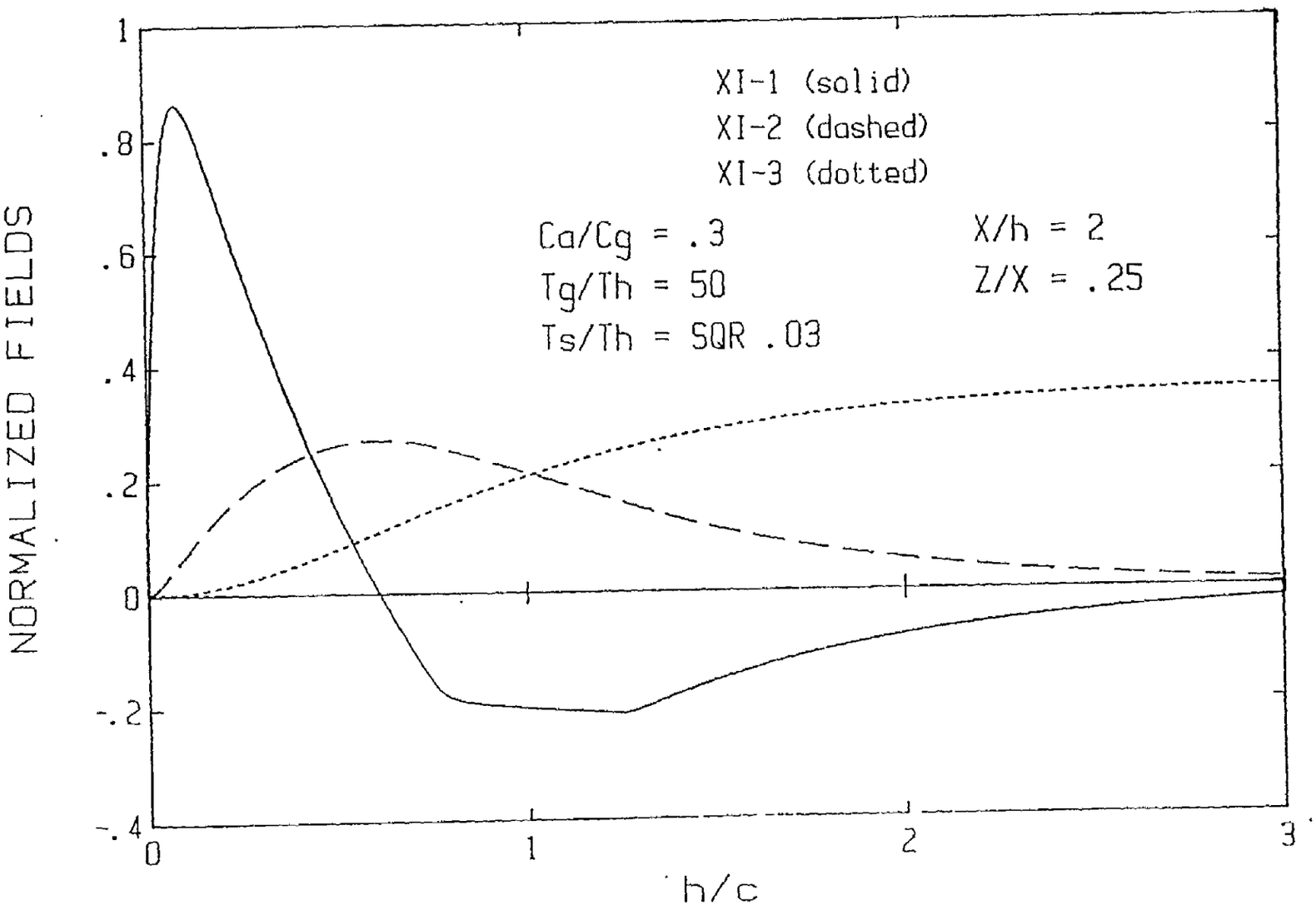

Figure 10. Normalized Field Components

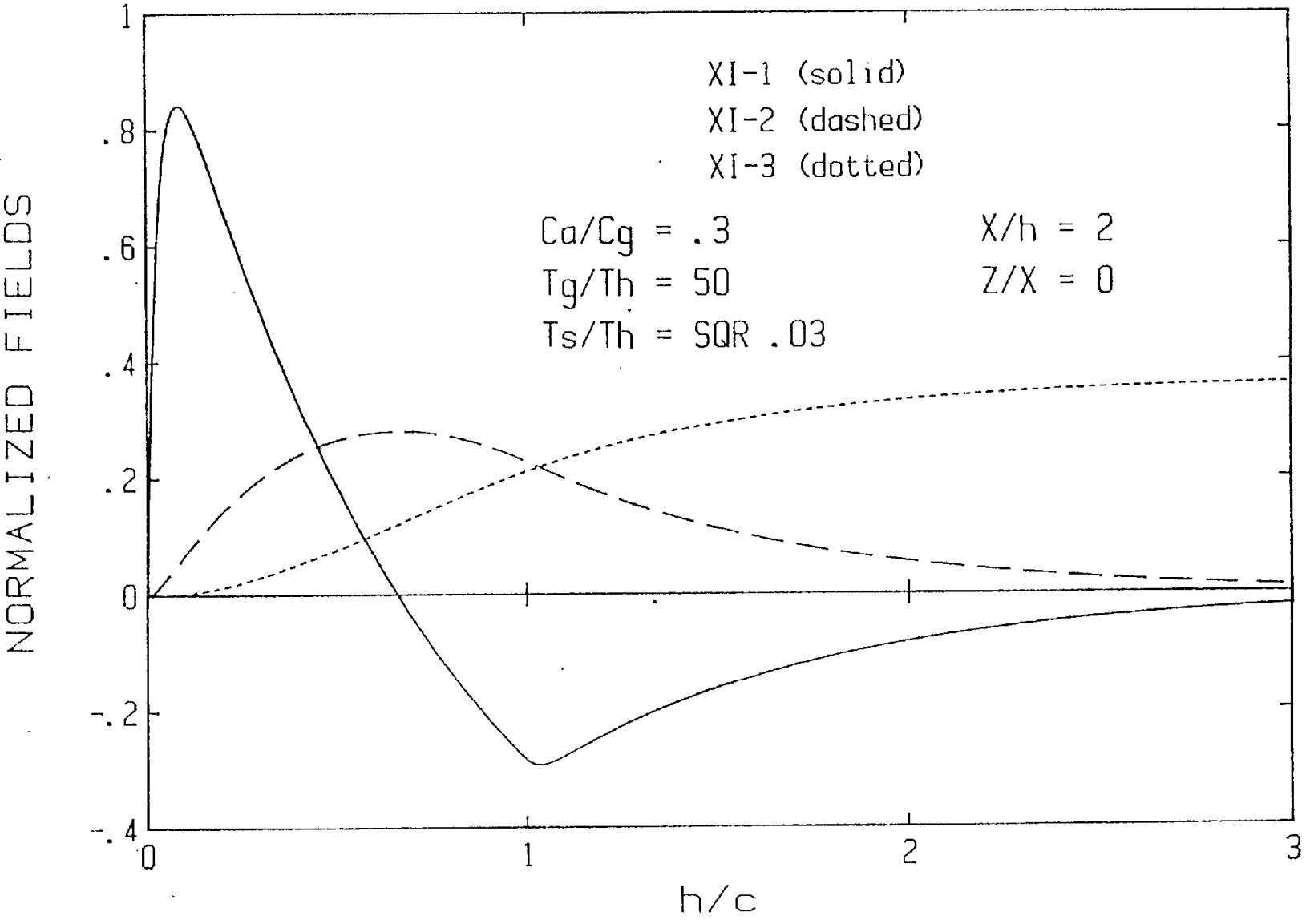

Figure 11. Normalized Field Components Above Ground Plane

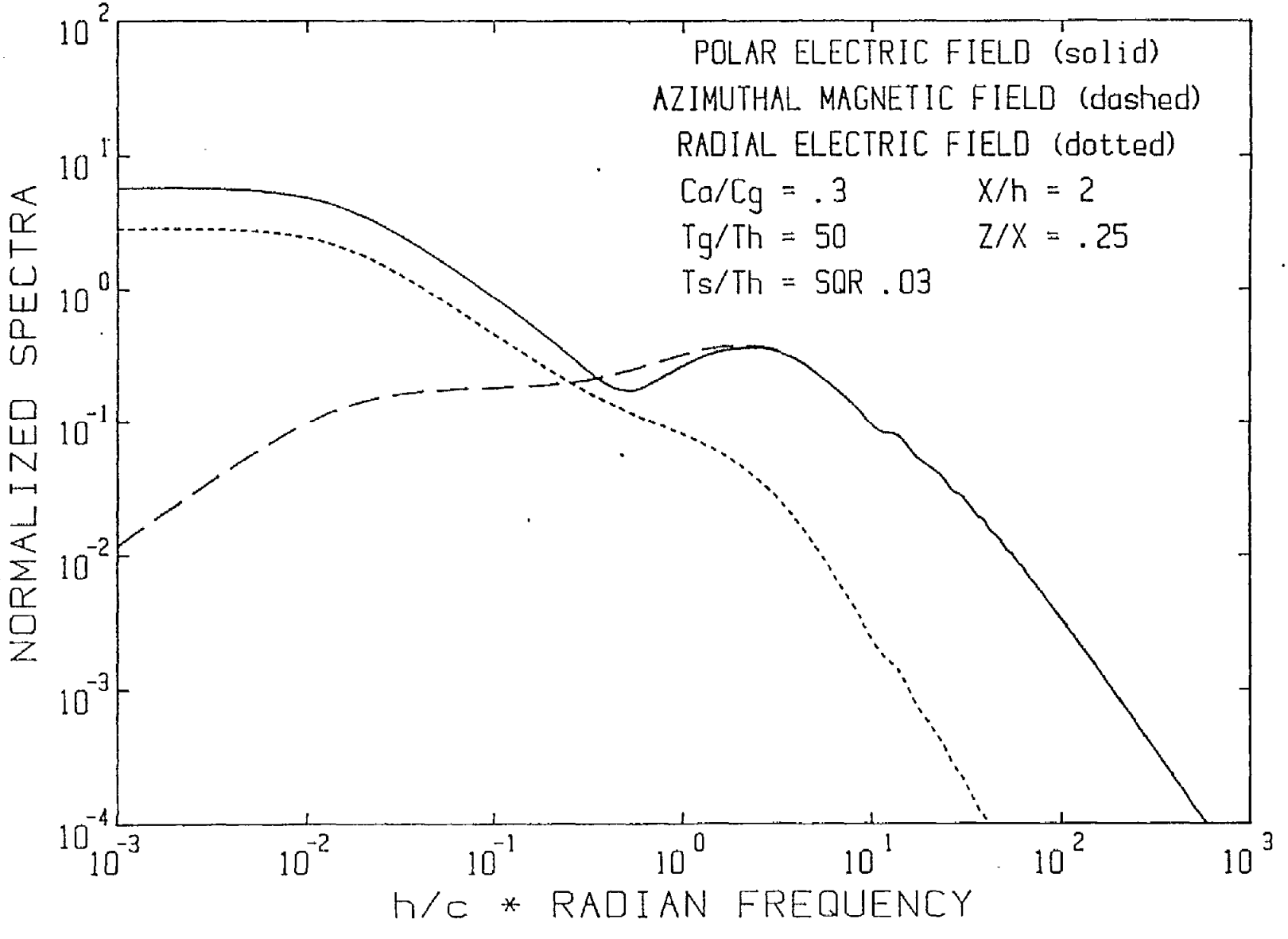

Figure 12. Spectra of Radiated Fields for Baseline Parameters

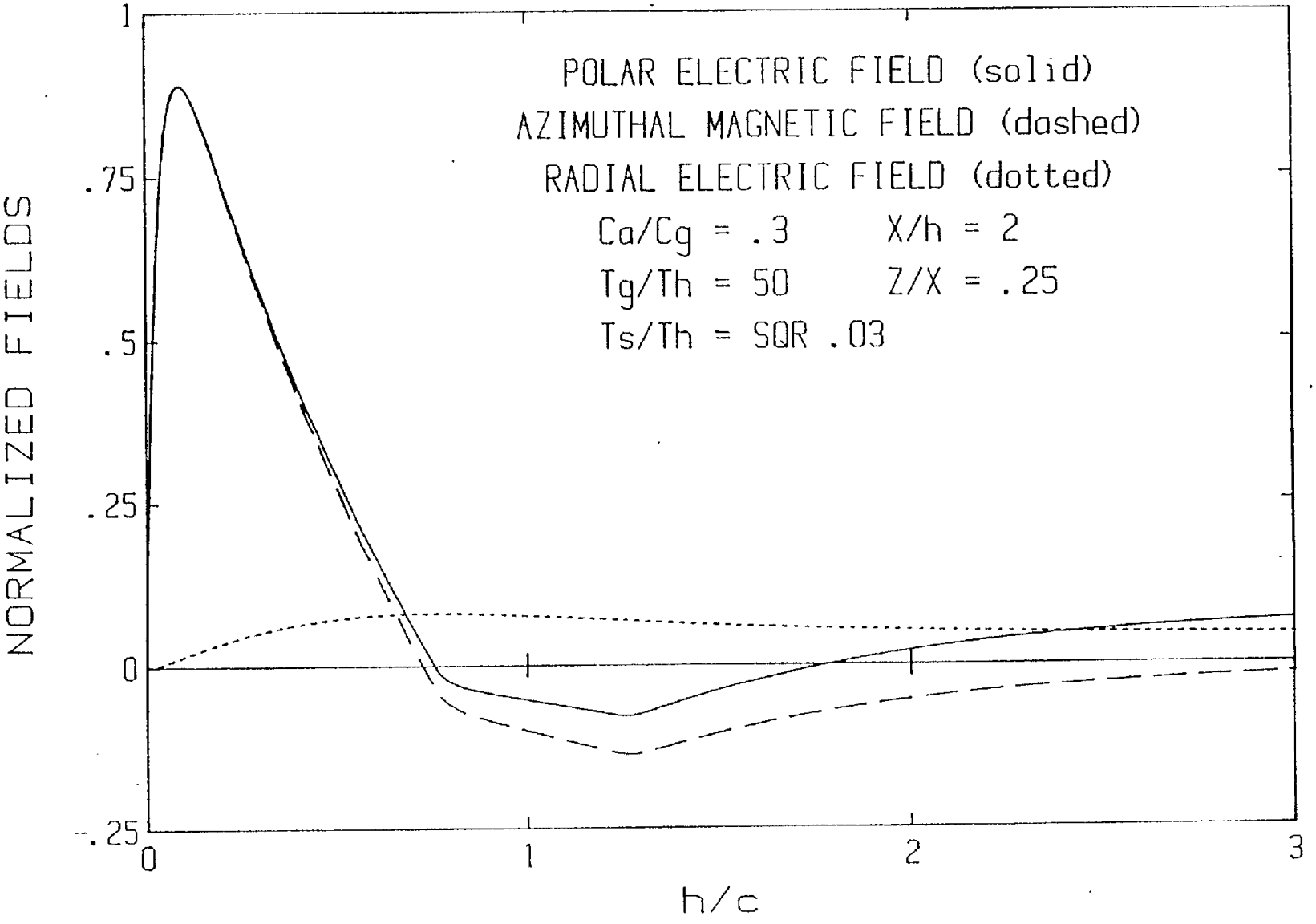

Figure 13. Radiated Fields for Baseline Parameters

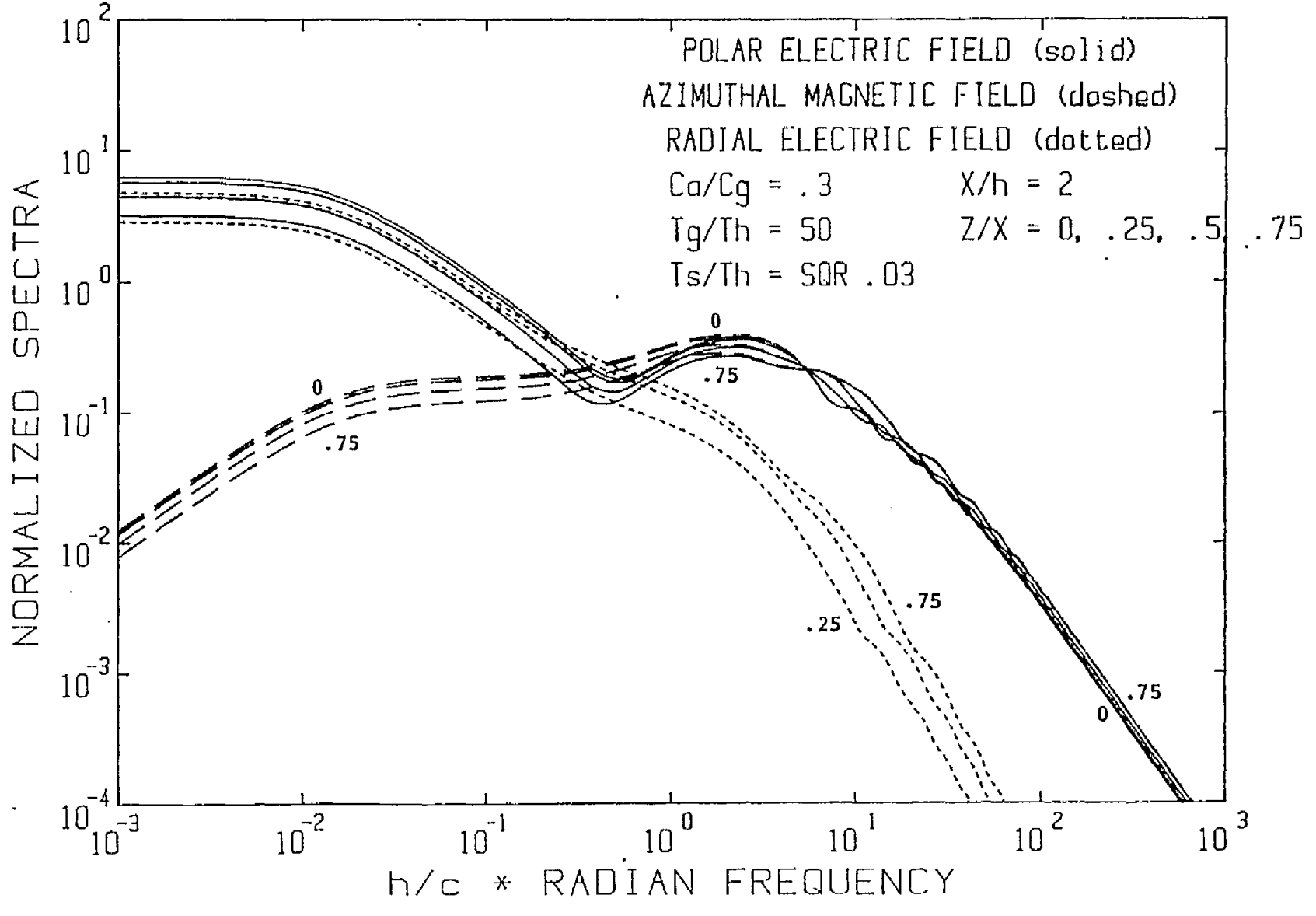

Figure 14. Variation of Spectra with Test Point Elevation

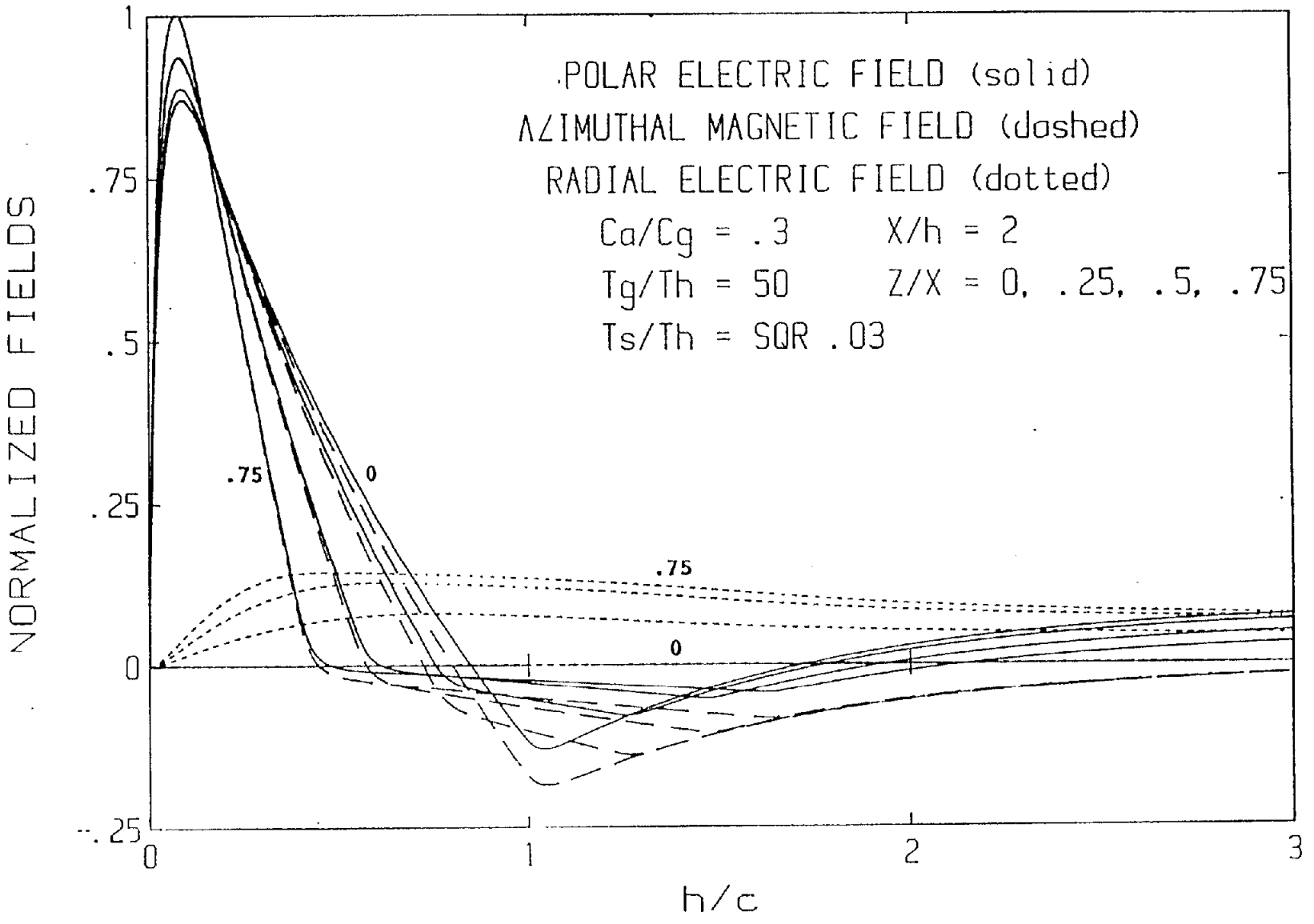

Figure 15. Variation of Fields with Test Point Elevation

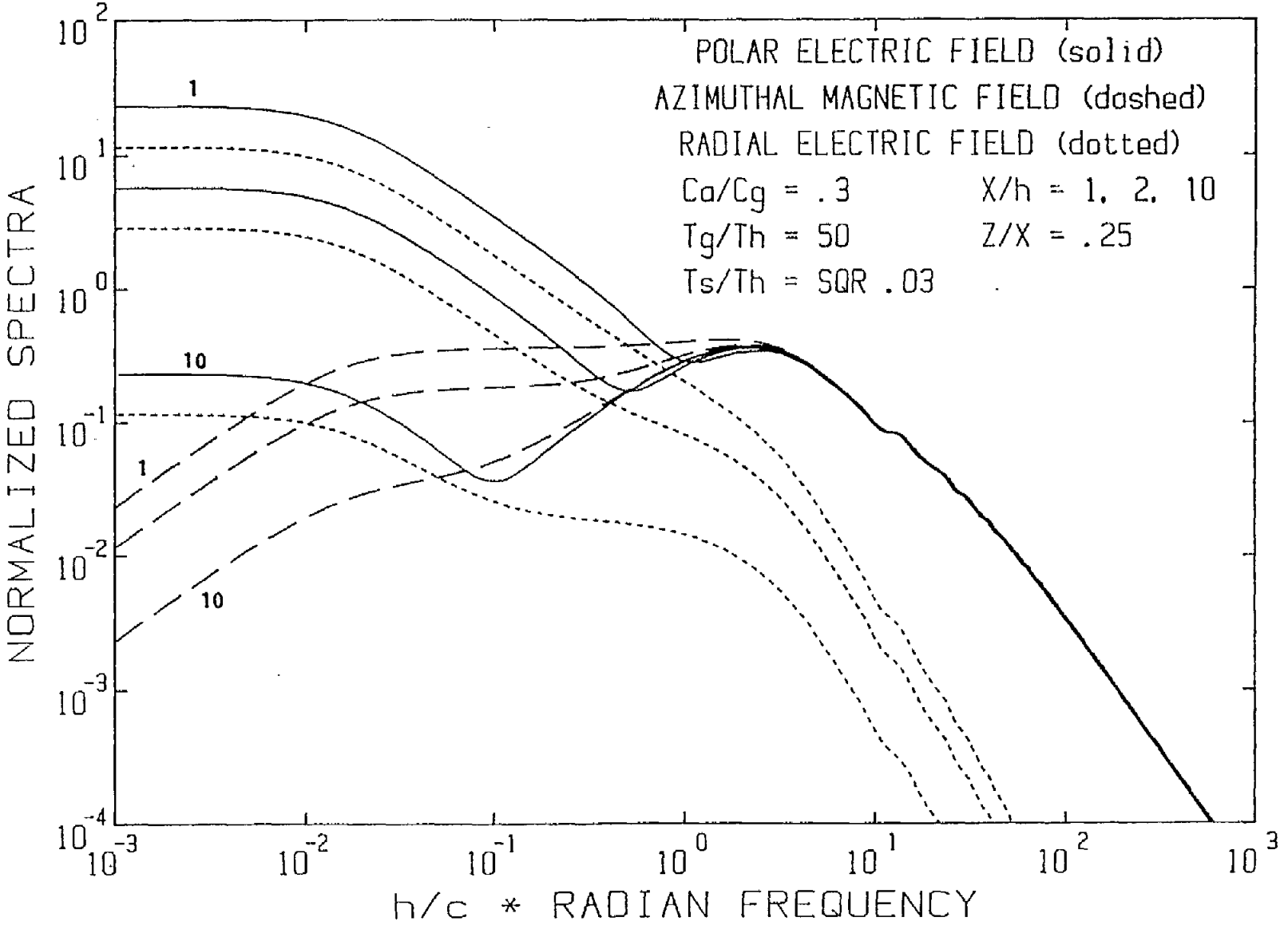

Figure 16. Effect of Distance on the Radiated Fields

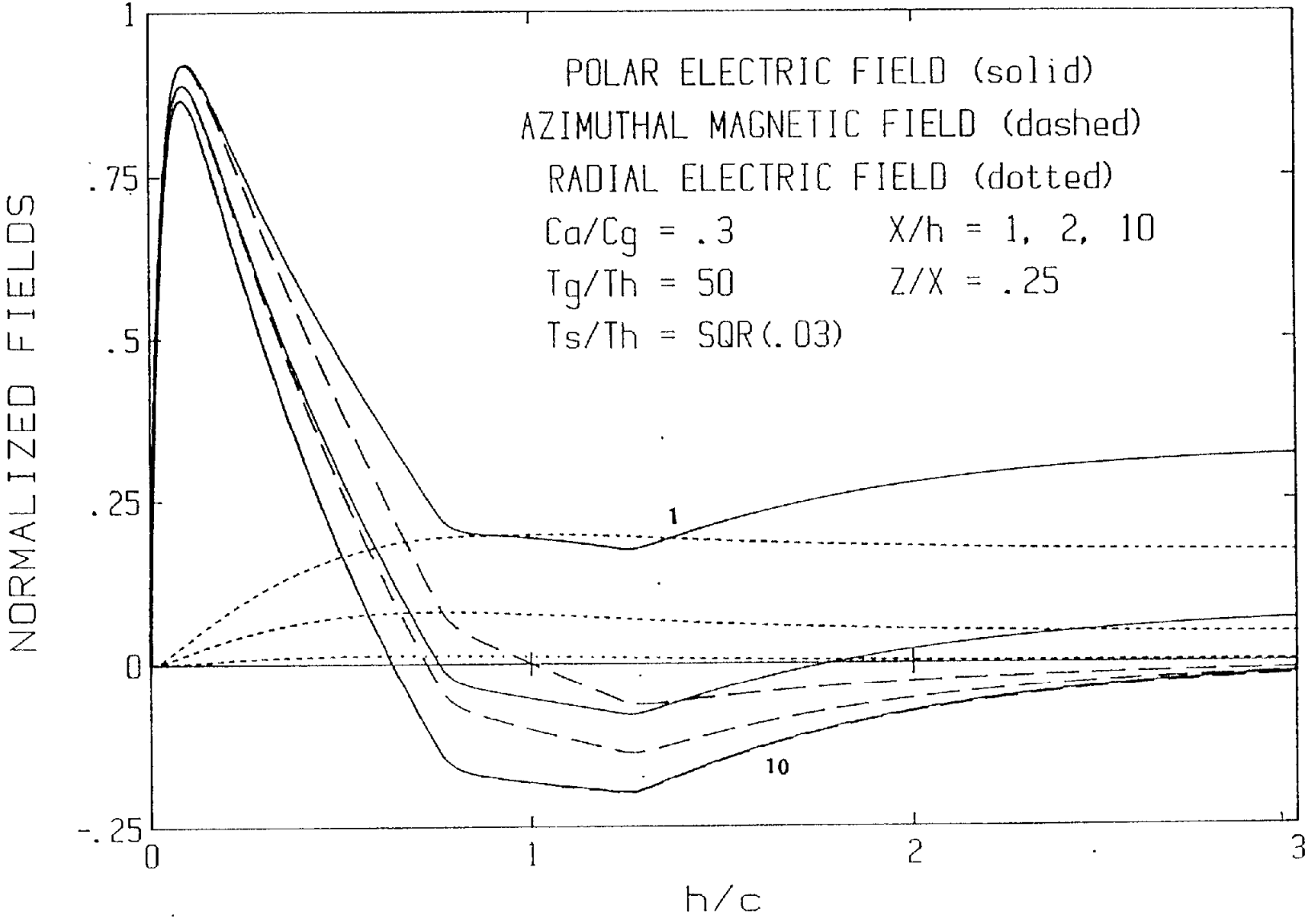

Figure 17. Effect of Distance on the Radiated Spectra

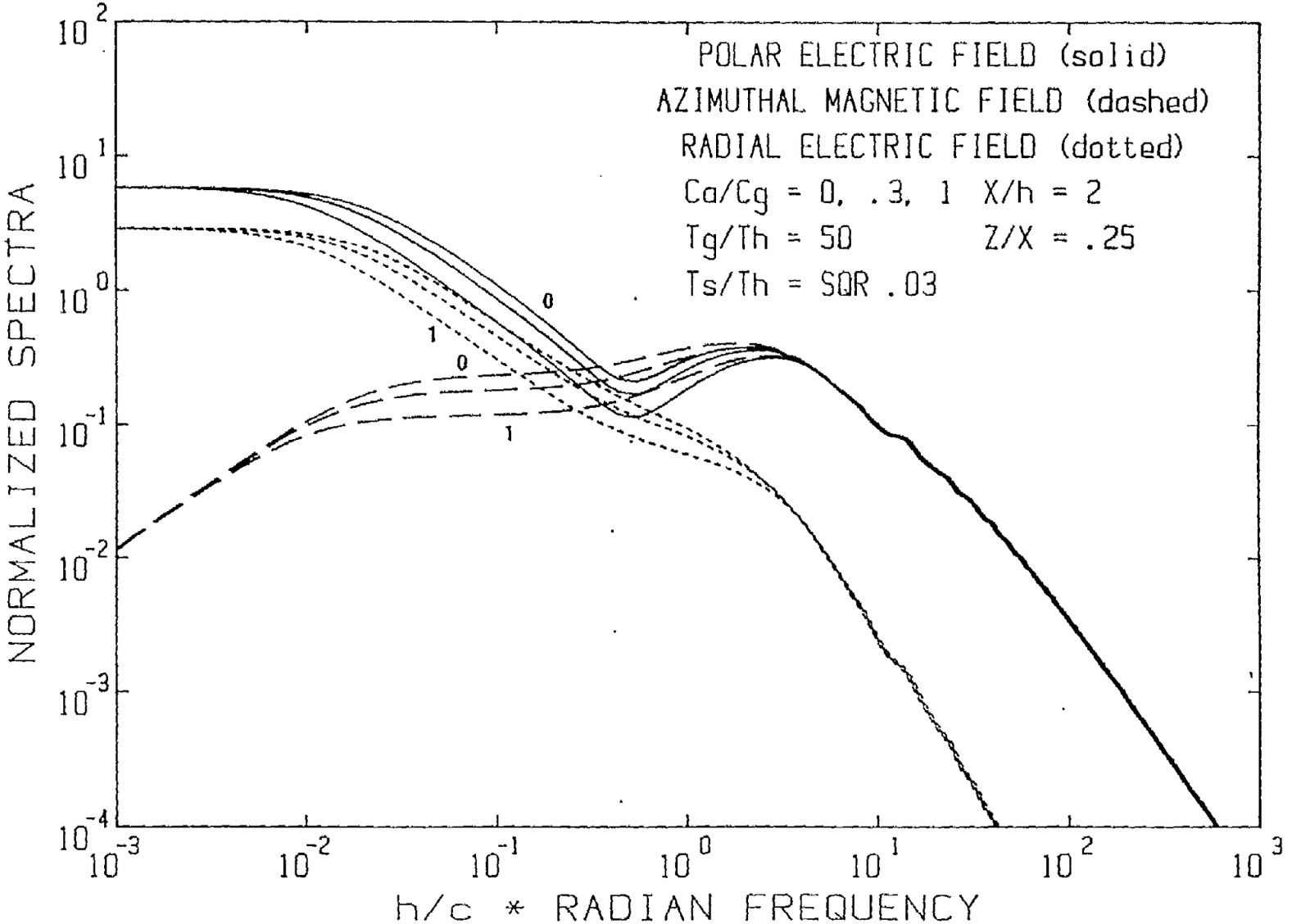

Figure 18. Effect of Antenna/Pulser Capacitance

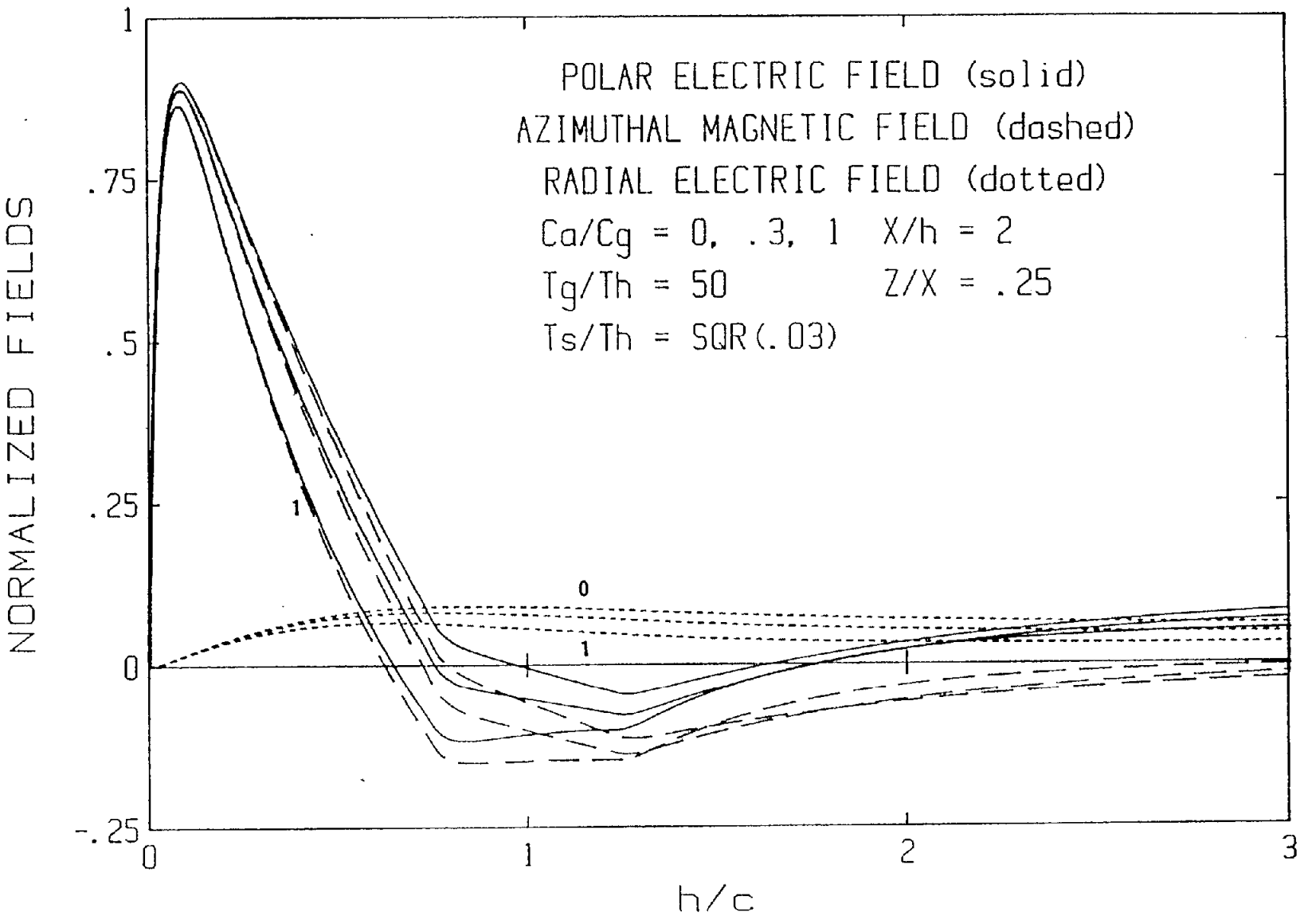

Figure 19. Effect of Antenna/Pulser Capacitance

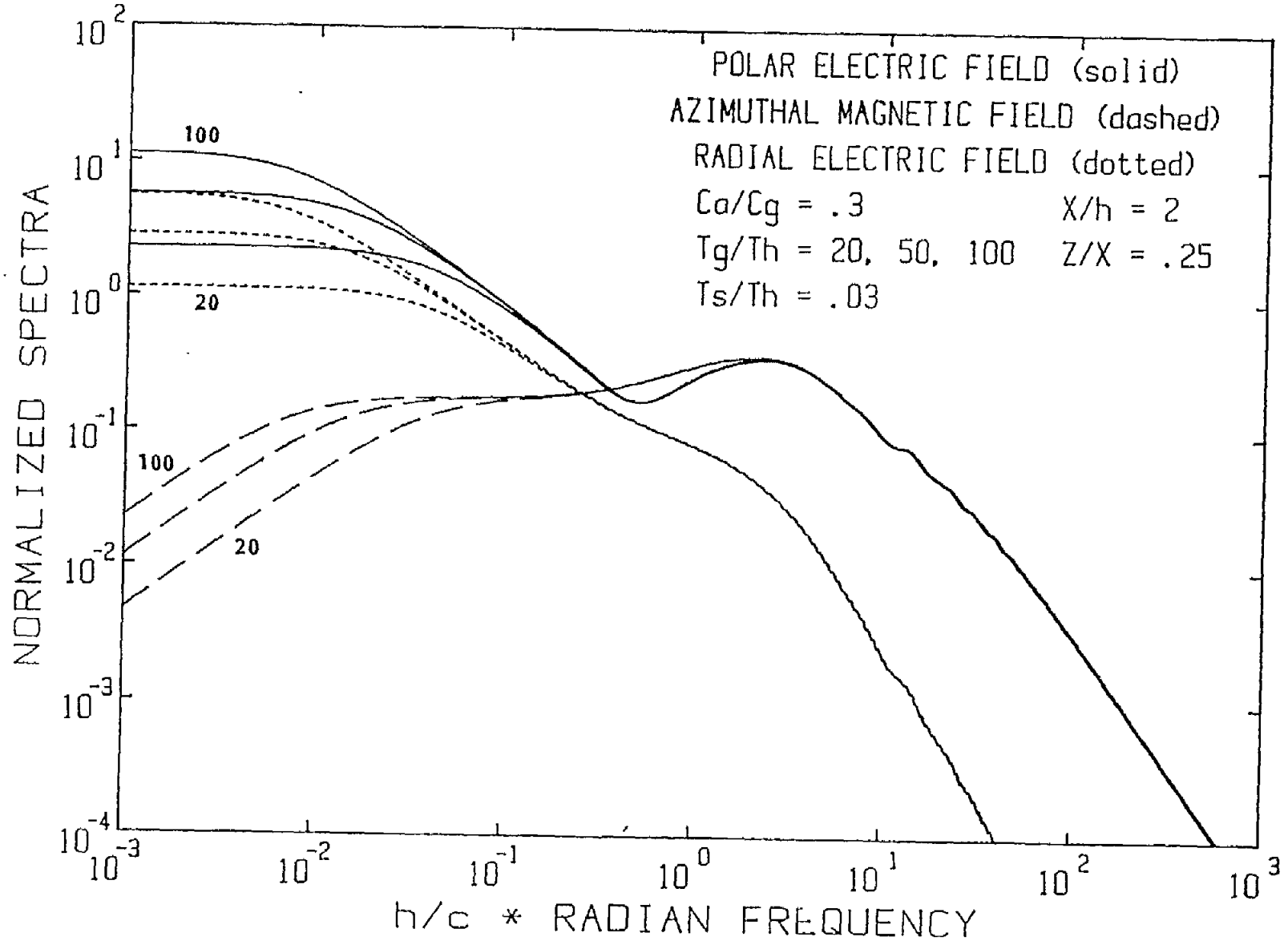

Figure 20. Effect of Pulser Shunt Resistance

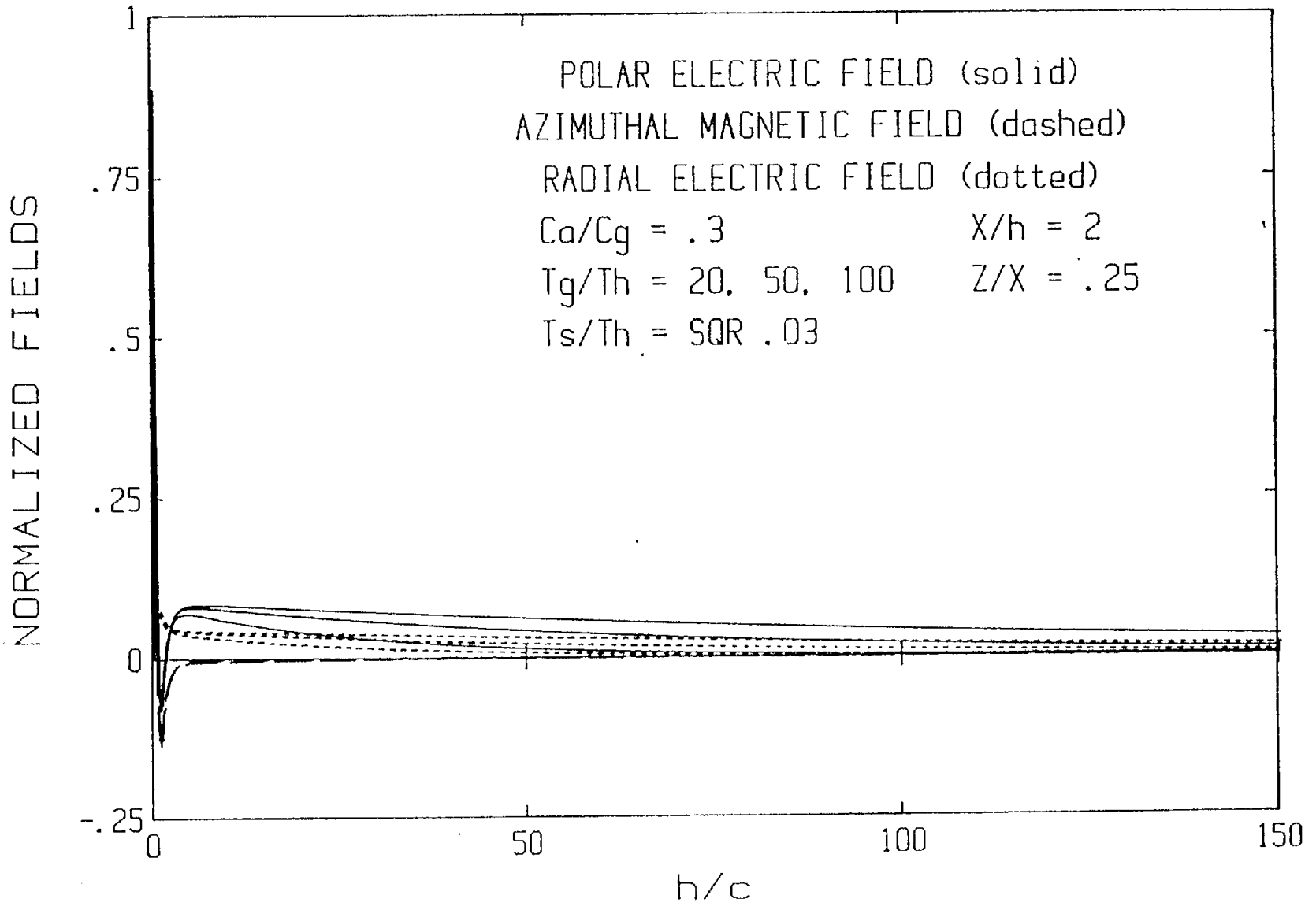

Figure 21. Effect of Pulser Shunt Resistance

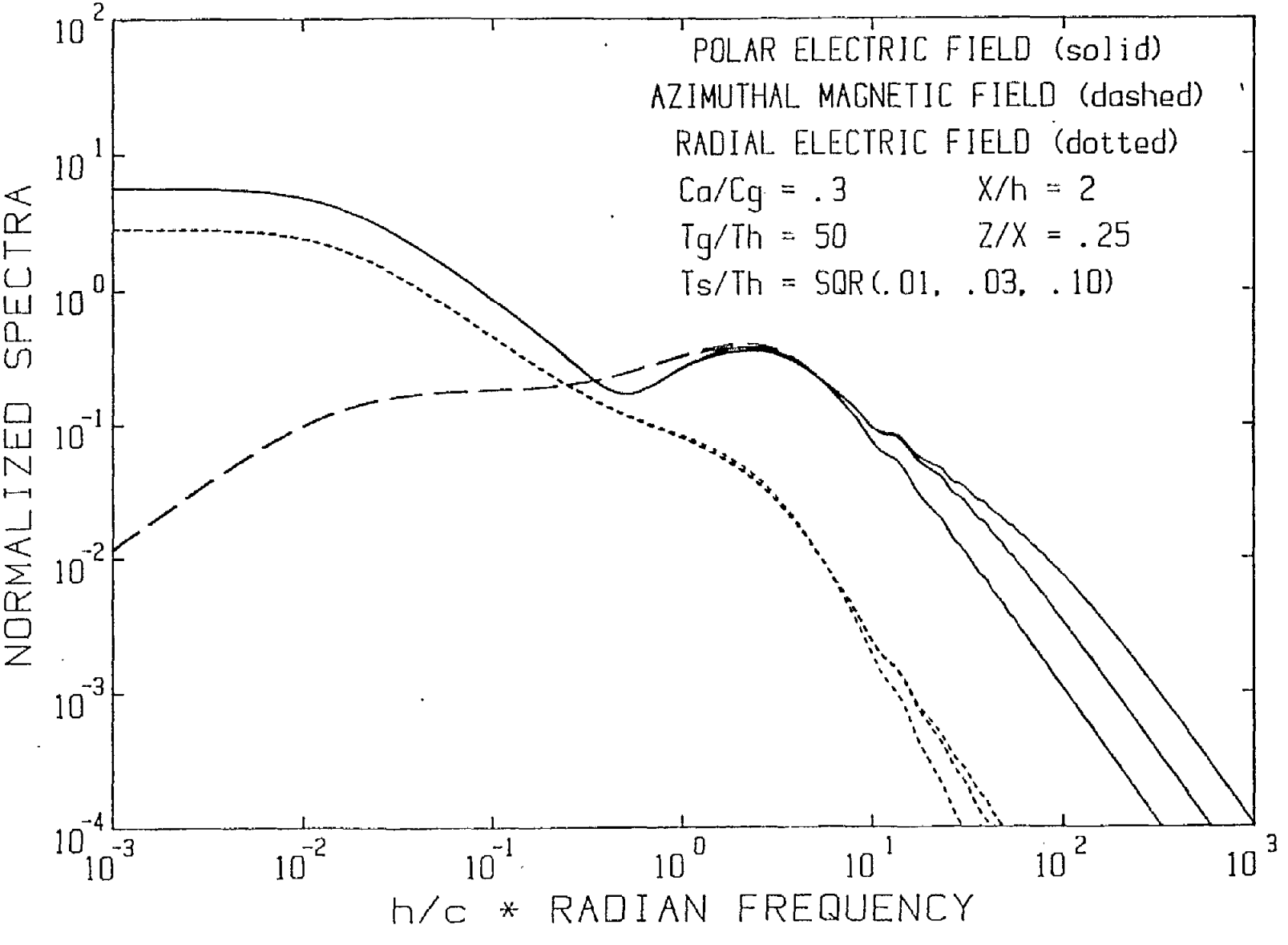

Figure 22. Effect of Output Switch Inductance

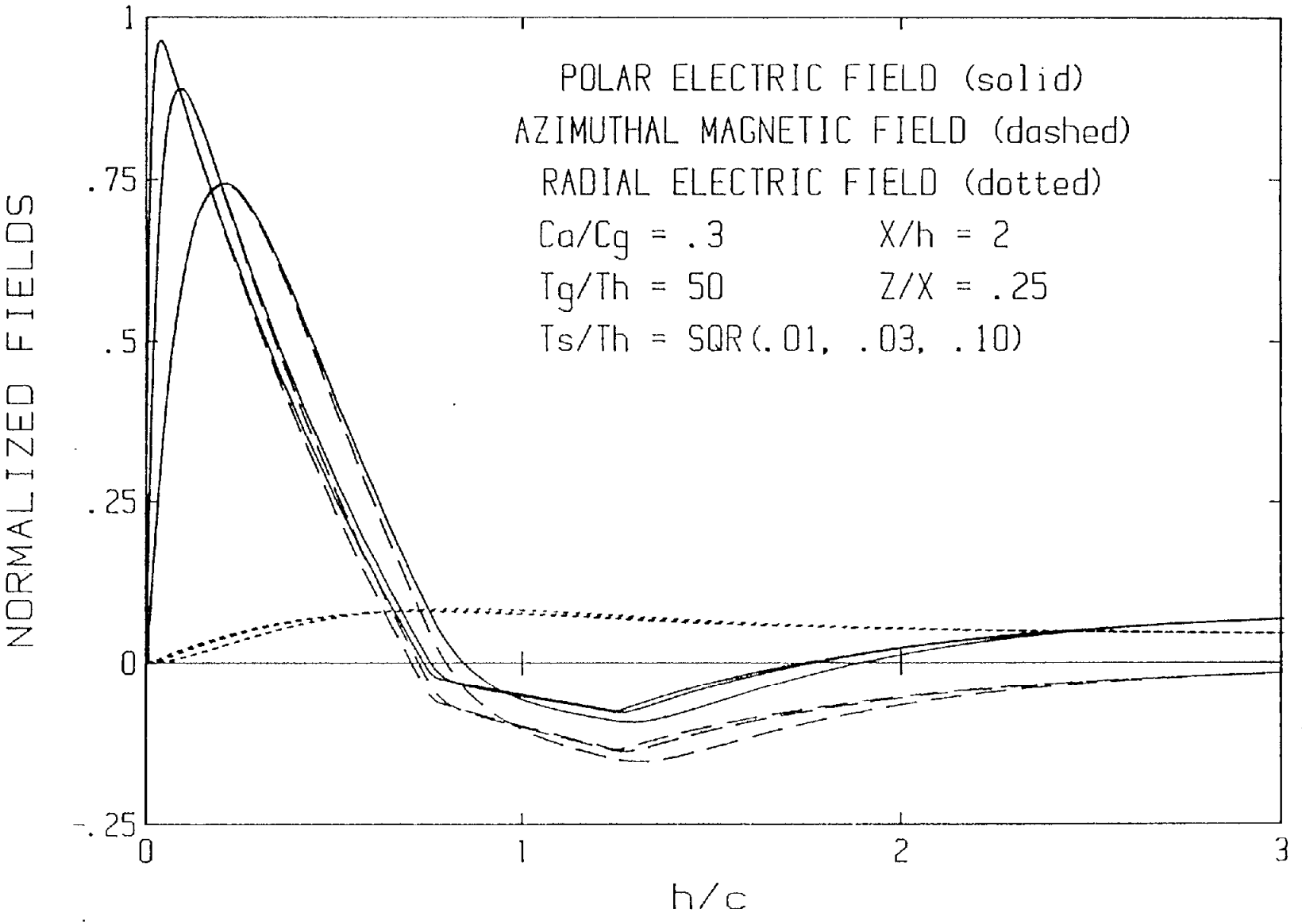

Figure 23. Effect of Output Switch Inductance